SCIENCE CHINA
Physics, Mechanics & Astronomy

• Invited Review •

October 2022 Vol. 65 No. 10: 104201
https://doi.org/10.1007/s11433-022-1957-3

Emerging material platforms for integrated microcavity photonics

Jin Liu[1†], Fang Bo[2†], Lin Chang[3†], Chun-Hua Dong[4†], Xin Ou[5†], Blake Regan[6†], Xiaoqin Shen[7†], Qinghai Song[8†], Baicheng Yao[9†], Wenfu Zhang[10†], Chang-Ling Zou[4†], and Yun-Feng Xiao[11†]

[1] *State Key Laboratory of Optoelectronic Materials and Technologies, School of Physics, Sun Yat-sen University, Guangzhou 510000, China;*
[2] *MOE Key Laboratory of Weak-Light Nonlinear Photonics, TEDA Institute of Applied Physics and School of Physics, Nankai University, Tianjin 300071, China;*
[3] *State Key Laboratory of Advanced Optical Communications System and Networks, School of Electronics, Peking University, Beijing 100871, China;*
[4] *CAS Key Lab of Quantum Information, University of Science and Technology of China, Hefei 230026, China;*
[5] *State Key Laboratory of Functional Material for Informatics, Shanghai Institute of Microsystem and Information Technology, Chinese Academy of Sciences, Shanghai 200050, China;*
[6] *School of Mathematical and Physical Sciences, University of Technology Sydney, Ultimo 2007, Australia;*
[7] *School of Physical Science and Technology, ShanghaiTech University, Shanghai 201210, China;*
[8] *Ministry of Industry and Information Technology Key Lab of Micro-Nano Optoelectronic Information System, Harbin Institute of Technology, Shenzhen 518055, China;*
[9] *Key Laboratory of Optical Fiber Sensing and Communications (Ministry of Education), University of Electronic Science and Technology of China, Chengdu 611731, China;*
[10] *State Key Laboratory of Transient Optics and Photonics, Xi'an Institute of Optics and Precision Mechanics, Chinese Academy of Sciences, Xi'an 710119, China;*
[11] *State Key Laboratory for Mesoscopic Physics and Frontiers Science Center for Nano-optoelectronics, School of Physics, Peking University, Beijing 100871, China*

Received May 5, 2022; accepted July 19, 2022; published online September 1, 2022

Many breakthroughs in technologies are closely associated with the deep understanding and development of new material platforms. As the main material used in microelectronics, Si also plays a leading role in the development of integrated photonics. The indirect bandgap, absence of $\chi^{(2)}$ nonlinearity and the parasitic nonlinear absorptions at the telecom band of Si imposed technological bottlenecks for further improving the performances and expanding the functionalities of Si microcavities in which the circulating light intensity is dramatically amplified. The past two decades have witnessed the burgeoning of the novel material platforms that are compatible with the complementary metal-oxide-semiconductor (COMS) process. In particular, the unprecedented optical properties of the emerging materials in the thin film form have resulted in revolutionary progress in microcavity photonics. In this review article, we summarize the recently developed material platforms for integrated photonics with the focus on chip-scale microcavity devices. The material characteristics, fabrication processes and device applications have been thoroughly discussed for the most widely used new material platforms. We also discuss open challenges and opportunities in microcavity photonics, such as heterogeneous integrated devices, and provide an outlook for the future development of integrated microcavities.

microcavity, integrated optics, nonlinear optics

PACS number(s): 47.55.nb, 47.20.Ky, 47.11.Fg

† Jin Liu, email: liujin23@mail.sysu.edu.cn; Fang Bo, email: bofang@nankai.edu.cn; Lin Chang, email: linchang@pku.edu.cn; Chun-Hua Dong, email: chunhua@ustc.edu.cn; Xin Ou, email: ouxin@mail.sim.ac.cn; Blake Regan, email: Blake.Regan@uts.edu.au; Xiaoqin Shen, email: shenxq@shanghaitech.edu.cn; Qinghai Song, email: qinghai.song@hit.edu.cn; Baicheng Yao, email: yaobaicheng@uestc.edu.cn; Wenfu Zhang, email: wfuzhang@opt.ac.cn; Chang-Ling Zou, email: clzou321@ustc.edu.cn; Yun-Feng Xiao, email: yfxiao@pku.edu.cn

Citation: J. Liu, F. Bo, L. Chang, C.-H. Dong, X. Ou, B. Regan, X. Shen, Q. Song, B. Yao, W. Zhang, C.-L. Zou, and Y.-F. Xiao, Emerging material platforms for integrated microcavity photonics, Sci. China-Phys. Mech. Astron. **65**, 104201 (2022), https://doi.org/10.1007/s11433-022-1957-3

1 Introduction

Optical microcavities can confine light to the sub-wavelength scale, thus dramatically enhancing light field intensity and significantly prolonging photon lifetime [1-4]. The strongly enhanced strength of light matter interactions in optical microcavities has been widely exploited for both exploring fundamental optical physics and developing functional photonic devices. The concept of spontaneous symmetry breaking, widely explored in high energy and condensed matter physics [5-8], has been established in optics, which brings new insights into the chaotic behavior of light transportation in asymmetric microcavities. Microcavities made of III-V compound semiconductors enable compact laser devices with low-power consumption for long-distance data transport over optical fiber networks. In the quantum regime, optical microcavities can enhance the emission rates of isolated two-level-systems, e.g., quantum dots and atoms for generating highly efficient non-classical light sources in the weak coupling regime, and even enable single-photon manipulations and quantum logic gates when reaching the strong coupling regime [9-12].

The realization of on-chip, integrated microcavities is particularly appealing due to the compatibility with the complementary metal-oxide semiconductor (CMOS) processes, the ability of mass production, the compact device sizes, and the low power consumption. A representative example is the microcavity fabricated on the silicon on insulator (SOI) platform. Thanks to the high-quality factors and the small mode volumes of the silicon (Si) microcavities, high-performance functional devices operating at the telecom band such as Raman lasers [13, 14], high-speed modulator [15, 16] and large bandwidth detectors [17-19] have been realized on integrated photonic chips. Si-based microcavities also have their own limitations that are intrinsically associated with the material properties. The indirect bandgap of Si severely limits the light emission efficiency, preventing the development of highly-efficient light sources on-chip. The centro-symmetric crystalline structure of Si results in the absence of the even-order optical nonlinearities, which makes it difficult to harness the most efficient second-order nonlinear optical processes such as cavity-enhanced second harmonic generations. Moreover, the parasitic free carrier absorption and two-photon absorption at the telecom band prevent high-optical power handling which is essential for achieving appreciable third-order nonlinear optical processes in Si. In addition, other desirable optical properties for more advanced integrated photonic devices, e.g., piezoelectric effect and transparency in the visible wavelength ranges, are highly desirable yet not available in Si. Therefore, tremendous efforts have been made during the past two decades to develop new material platforms for integrated microcavities with improved device performances and expanded functionalities.

The implementations of large bandgap materials in the thin film geometry, such as doped silica, silicon nitride (SiN), aluminum nitride (AlN), silicon carbide (SiC), diamond, and lithium niobite (LN), have successfully extended the spectrum of microcavity photonics into the visible wavelength ranges. In addition, the strong electro-optic effect in LN and the piezoelectric effect in AlN enable the realization of functional devices, e.g., fast electro-optic modulators and acoustic wave transducers that are not achievable in Si. The ultra-low optical loss and engineerable dispersion provided by SiN microresonators make the soliton microcombs routinely accessible without high-power pumping with optical amplifiers. The development of aluminum gallium arsenide (AlGaAs) on insulator (AlGaAsOI) platform simultaneously brings optical gain and large optical nonlinearities into the integrated photonics while avoiding the two-photon absorption at C-band that limits the high-power operations in Si microcavities. As a highly-efficient gain material, halide perovskite is becoming increasingly important when making photovoltaic and light emitting devices due to the low-cost synthesis and high quantum yield. Last but not least, introducing atomically thin materials such a two-dimensional (2D) layered material and single layers of molecules on the surfaces of microcavities provides exciting opportunities of expanding the functionalities and improving the device performances of the existing Si microcavities. This review mainly covers the recently emerging material platforms for planar microcavities, while many other promising materials are not discussed here, including plasma materials, III-V materials such as GaAs and InP, rare-earth ions implanted into various substrates, and silicate glasses.

In this review, we summarize the recently developed thin film material platforms for integrated photonics with the focus on microcavity devices, covering doped silica, SiN, AlN, SiC, diamond, LN, AlGaAs, halide perovskite, and 2D materials and organic molecules. For each of these materials, we start with an introduction of its basic optical properties, followed by a discussion of the scalable fabrication techniques of high-quality planar microcavities, and highlight the unique device applications with the focus on on-chip light sources

and nonlinear photonics. Finally, we discuss the opportunities and on-going progress on hybrid integrated platforms that take advantage of different material systems for future advanced microcavity devices as a whole.

2 Doped silica

High-index doped silica (refractive index range of n=1.5-1.9) is particularly promising due to its low linear loss (propagation loss of 1-6 dB/m), relatively large nonlinearities (n_2 = 1.15×10^{-19} m^2 W^{-1}, approximately 4.5 times higher than silica and half of SiN), and negligible nonlinear loss in telecom band (without multi-photon absorption) [20-23]. Many studies based on this material platform have been explored due to its favorable optical performance, CMOS-compatible fabrication process and high material stability. Early investigations mainly focused on linear waveguides and microring resonators (MRRs) for large-scale photonic integrated circuits such as Mux/Demux wavelength division multiplexing (WDM) filters using MRR arrays [24]. In last decade, high-index doped silica has achieved considerable success in the area of nonlinear optics as well, such as supercontinuum generation [25] , pulse compression [26] using a long spiral waveguide, and especially microcombs (or Kerr combs) generated by high-Q MRRs [27].

Typical fabrication processes of doped silica microcavities contain thin film deposition using chemical vapor deposition (CVD), circuit print in photoresist with projection stepper lithography and pattern transfer by reactive ion etching (RIE). Figure 1(a) and (b) show scanning electron microscope (SEM) images of a single waveguide for external input/output and coupled waveguides for energy exchange, respectively, where the waveguide cores are usually with 1-3 μm both of width and height. Figure 1(c) shows a spiral waveguide over 1 m length which has been used for the stimulated Brillouin scattering experiment [28]. Figure 1(d) shows a four-port doped silica MRR with a typical quality factor (Q-factor) of 2-4 million. Figure 1(e) and (f) exhibit a sample pigtailed with a standard fiber array at low coupling loss and butterfly packaged with a commercial thermoelectric cooler, respectively. Taking advantages of the mature developing process of doped silica material, thousands of MRRs can be fabricated simultaneously in a 6-inch wafer as depicted in Figure 1(g).

After the first demonstration of optical parametric oscillation [29], this type of MRR has fully manifest itself as an attractive competitor for nonlinear optics, including all-optical wavelength conversion [30], narrow-bandwidth pulse mode-locking [31], third-harmonic generation [32] and Raman self-frequency-shift [33]. Especially in the field of microcombs (Figure 1(h)) other than the soliton crystal state [33,34], the single dissipative Kerr soliton (DKS) generation is considered as a long-lasting challenge towards wide applications [35], due to the difficulty to overcome system thermal instability, however, has been achieved by high-Q MRRs, benefitting from its easy controllability on operation temperature. By introducing an auxiliary laser counter-coupled to the pump, deterministic DKS generation and switching was successfully obtained [36]. Furthermore, through adopting the microcomb power as the criteria for state discrimination, program-controlled single soliton microcomb source with one-button start capacity has also been realized [37]. Other remarkable progress includes self-locked dual-comb generation [38], soliton burst and bi-directional switching [39], repetition-rate control assisted by temporal Talbot effect [40], and synthesized soliton crystal with ordered temporal distribution [41].

Until now, the high-index doped silica glass MRR-based microcombs have been utilized as proof-of-concept in various applications. Representative examples, including Hilbert transformers [42], adaptive photonic RF filters [43], and arbitrary waveform generators [44], have been demonstrated for applications in microwave photonics. Regarding to the precision measurement, high-speed long-distance (~ 1179 m) ranging through the dispersive interferometry method based on soliton microcomb was achieved with a minimum Allan deviation of 27 nm [45]. For applications in optical communications, ultra-high data transmission (bit rate of 44.2 Tbps) over a 75 km standard fiber was obtained using soliton

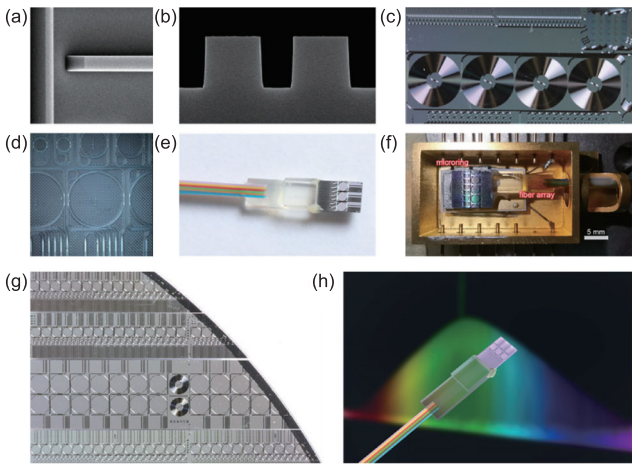

Figure 1 (Color online) High-index doped silica glass MRRs and their applications. (a) SEM image of a single waveguide and (b) coupling region between the bus and microring waveguide; (c) optical microscope image of spiral waveguide over 1 m; (d) four-port high-Q MRRs; (e) directional coupling of MRRs with single-mode fiber array; (f) butterfly-packaged MRR with thermoelectric cooler [45]; (g) optical image of a wafer containing thousands of MRRs; (f) concept image of soliton microcomb by doped silica MRR.

crystals [46]. In quantum optics, by using coherent microcomb lines as the light source for a quantum key distribution system, a secure key rate of ~200 kbps for one channel, with the potential of reaching Gbps via multiplexing technique, was demonstrated [47]. Additionally, these doped silica MRRs were verified to be capable of generating multiphoton and high-dimensional entangled quantum states, as well as the d-level cluster state for one-way quantum processing [48]. They can even find important role in a universal vector convolutional accelerator operating at a 11 Tops for optical neural networks [49]. All these achievements indicate that high-index doped silica glass MRRs are powerful candidates for practical and future-oriented applications across the classic and non-classic optics, thanks to their unique compatibility and excellent robustness.

3 SiN

Among various material platforms developed in the past decade, SiN has become the most attractive platform particularly for integrated nonlinear photonics, due to its large transparent window, absence of two-photon absorption in the telecommunication band, strong Kerr nonlinearity, high power handling capability and especially ultra-low optical losses (1 dB/m) [50].

Soliton microcomb is one of the most popular fields for integrated nonlinear photonics in recent years. SiN has emerged as the leading platform for soliton microcomb due to its ultra-low linear and nonlinear losses (Figure 2(a)) [51]. Many phenomena such as dissipative Kerr soliton [52-54], dispersive wave [55], breathing solitons [56, 57] and soliton crystals [58] and applications such as optical clock [59], ultrafast ranging [60] and microwave generation [61] have been demonstrated based on SiN microresonators. Benefiting from recent advances in fabrication process of SiN photonic integrated circuits (PICs), intrinsic quality factor for on-chip SiN microresonators has exceeded 3×10^7, which reduces the on-chip pump power required for soliton generation to a few milliwatts [62]. With such low pump power for soliton generation, recent studies have demonstrated that the turnkey soliton microcomb can be generated by the hybrid (Figure 2(b)) or heterogeneous (Figure 2(c)) integrated system of indium phosphide (InP) laser and SiN microresonators by using the self-injection locking technique [63, 64], which greatly simplifies the soliton microcomb system and reveals the viability of fully chip-based soliton microcombs.

Besides the soliton microcomb, SiN also shows its advantages of ultra-low linear and nonlinear losses and strong Kerr nonlinearity in other nonlinear photonic devices. Figure 2(d) shows the optical amplifiers which are essential in numerous photonic applications. Based on the 1.42-m-long SiN waveguide with the propagation loss of 1.4 dB/m, the first on-chip continuous-wave parametric amplification with the gain of 9.5 dB was achieved [65]. Moreover, by appropriate dispersion engineering, the SiN waveguide can be used to generate the supercontinuum to extend the spectrum into the mid-infrared band, which is significant for molecular spectroscopy [66]. Furthermore, delicately engineered SiN nonlinear photonic devices are also required for quantum system. The generation of quantum random number and the strongly squeezed light are realized by two groups in 2021, respectively [67, 68], showing that the significant control can be achieved over quantum nonlinear optical processes by inte-

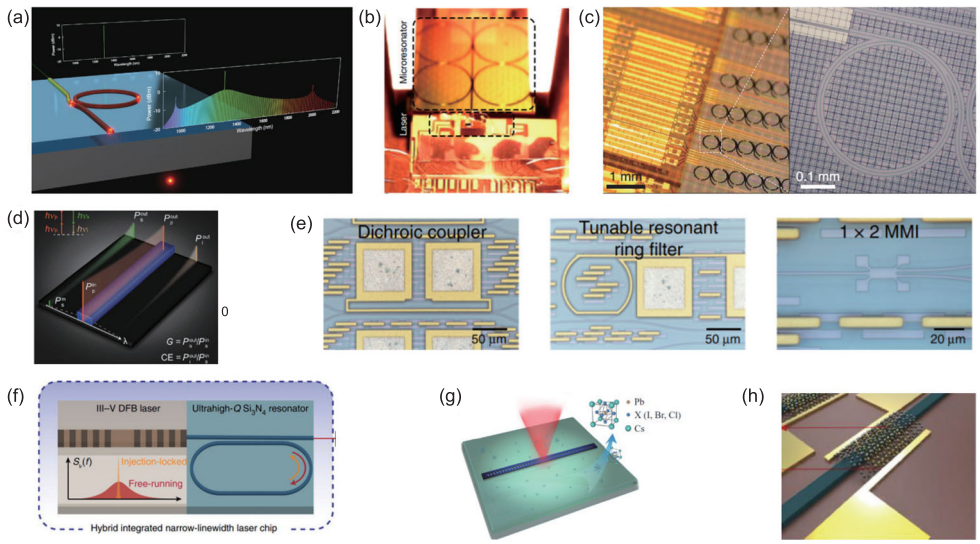

Figure 2 (Color online) Integrated photonics with silicon nitride. (a)-(c) Soliton microcomb based on silicon nitride platform [51, 63, 64]; (d) integrated SiN nonlinear photonic devices [65]; (e), (f) passive and active elements based on SiN [69, 71]; (g), (h) integrated SiN photonic devices with other materials [73, 75].

grated photonic platforms.

Since SiN is becoming an increasingly important platform for integrated photonics, plenty of active and passive elements based on SiN have been proposed and demonstrated in recent years, such as the ultra-narrow linewidth laser based on self-injection locking (Figure 2(f)) [69], the tunable photonic delay line [70], dichroic filters, tunable ring filters, multimode interferometers (Figure 2(e)) [71], and the thermo-optic phase modulator [72]. Moreover, by integrating with other materials, SiN PICs are endowed with extra features, for example, the high-performance coherent light resource composed of perovskite nanocrystals and the SiN nanobeam cavity (Figure 2(g)) [73], the magnetic-free optical isolator based on aluminium nitride (AlN) piezoelectric modulators and the SiN microring resonator [74], and the visible light detector consisting of the graphene/MoS_2 heterostructure and the SiN waveguide (Figure 2(h)) [75]. As more and more functions of bulk free-space and fiber-optic components can be replaced by PICs, fully integrated miniaturized optical systems based on SiN are expected to be realized.

4 AlN

AlN has been widely applied in microelectromechanical (MEMS) devices, due to its excellent mechanical properties and mature micro-/nano-fabrication technologies. AlN is also a wide bandgap (~6 eV) semiconductor, thus being optically transparent over a wide range of wavelengths from violet to infrared [76]. In addition, AlN possesses intrinsic second-order optical nonlinear susceptibilities. Therefore, AlN provides a versatile material platform for studying the light-matter interactions [77], including the nonlinear mixing between photon-photon, photon-microwave photon, and photon-phonon. Benefiting from the tight light field confinement and high optical Q, these interactions are greatly enhanced in AlN microcavities, and the potential of AlN in photonics beyond the limitations of conventional silicon-based materials have been revealed.

Figure 3 summarizes the various photonics devices based on AlN microcavities that have been demonstrated experimentally. First of all, the AlN is appealing for its nonlinearity (Figure 3(a)). By engineering the AlN microring that provides high-Q simultaneously at visible and telecom wavelengths, the high-efficient second-harmonic generation [78], optical parametric oscillation [79], and visible-to-telecom quantum frequency conversion [80] have been demonstrated. AlN also offers the nonlinearity for realizing the cascaded four-wave mixing and thus enables the mode-locked frequency comb generation with a beyond-octave spectral span [81, 82] (Figure 3(b)). Utilizing the electro-optics effect, the high-speed control and reconfiguration of AlN photonic devices, as well as the coherent three-wave mixing effect beyond the optical frequencies are enabled [83] (Figure 3(c)). Its excellent mechanical properties also allow the optomechanical devices at ultrahigh (~10 GHz) mechanical frequencies [84] (Figure 3(d)). In single-crystalline AlN, even the optical phonon has narrow linewidth, and thus low-threshold Raman lasing and cascaded Raman lasers are achieved [85] (Figure 3(e)).

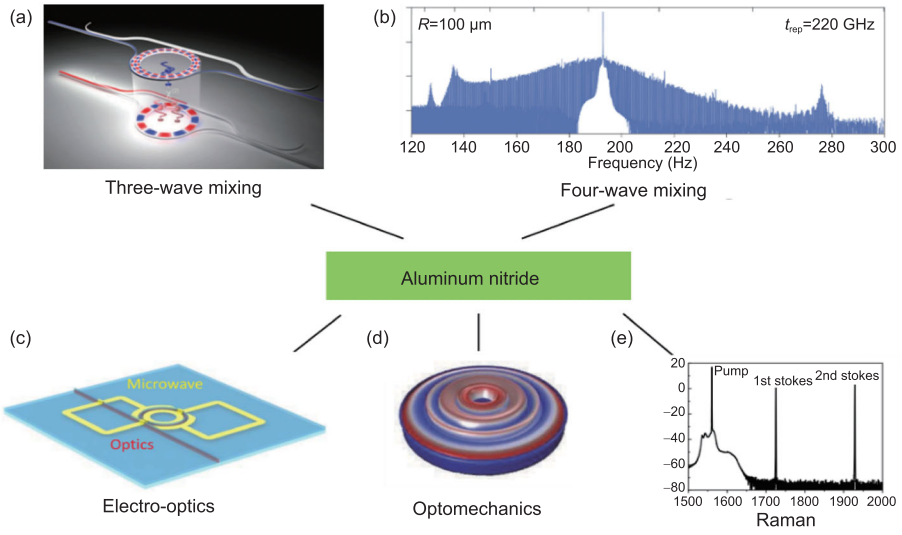

Figure 3 (Color online) Various photonic devices based on AlN microcavities. (a) The phase-matched three-wave mixing between 780 and 1550 nm optical modes in AlN microring [78]; (b) the beyond-octave optical soliton generation [81]; (c) the superconducting electro-optics device for optics-to-microwave frequency conversion [83]; (d) the high-frequency optomechanical microdisk cavity, with the mechanical mode frequencies as high as 10 GHz [84]; (e) the cascaded Raman lasing in AlN microring [85].

As the distinct nonlinear optics processes have been demonstrated in AlN, it is anticipated that novel functional photonic devices could be realized by hybridizing these processes within a single AlN microcavity. For instance, the cascaded and nonlinearities enable the generation of optical soliton comb at visible and telecom wavelengths simultaneously, by either pump by visible laser or telecom laser [86,87]. It is also demonstrated that a single AlN microring could simultaneously convert and amplify the optical signal from visible wavelength to telecom band [80]. Combining the optomechanical and piezo-mechanical effects [88,89], a new architecture of the hybrid superconducting-AlN photonic chip is demonstrated, which offers a useful approach for realizing the interfacing between the superconducting quantum chips and holds great potential for the quantum network and distributed quantum processing. AlN microcavities are also of great theoretical interests by providing a unique model involving various nonlinear processes and the multiple traveling wave modes, which provides a network of nonlinearly coupled modes and is potential for machine learning based on reservoir computing.

In addition to the hybrid AlN devices that worth further explorations, the integration of different devices on a single AlN chip might play important role in the long-term development of photonics. Especially, AlN is very important from the following two aspects: (1) the chip for stabilized optical sources. It is possible to utilize the second-harmonic generation and electro-optic modulation in AlN microring to realize the self-referenced or atom-referenced frequency comb [81], which would be useful for optical communciations and sensing. (2) The quantum photonic chip. In addition to passive devices, and also the quantum frequency converter and modulators, the AlN platform also provides single emitters [90] for the essential quantum resources of single-photon nonlinearity. Additionally, the AlN waveguide is also compatible with near-unity-efficiency superconducting single-photon detectors [91,92]. Therefore, AlN is unique for the potential monolithic integration of full-functional quantum photonic circuits.

5 SiC

SiC is gaining much attention as a viable platform for the photonics application. It exhibits a wide bandgap (3.26 eV for 4H polytype), a high refractive index (2.6 at 1550 nm), a wide transparent window (0.37-5.6 μm) [93], a Pockels effect, and strong second- and third-order optical nonlinearities [94]. Besides, SiC is also a CMOS-compatible semiconductor material and hosts a variety of spin qubits [95-97], which promises to achieve monolithic integration of quantum photonics and electronics with low costs. The above comprehensive properties may make SiC a strong competitor for a promising photonics platform.

For this purpose, tremendous efforts have been attracted to develop SiC photonic microresonators over the past decades [95, 98-100]. As a semiconducting polymorphic material with abundant polytypes, there exist 250 different polytypes but only 3C, 4H and 6H-SiC can be stably grown and commercially available for applying in optoelectronic devices. Pioneering photonic microresonators research mainly focused on epitaxial 3C-SiC or deposited SiC on Si [101]. At that period, the photonic microresonators were generally fabricated by undercutting the beneath substrate. With this configuration, the structures usually require a sophisticated process, which makes the fabrication inconvenient. Compared with the epitaxial or deposition technique, a practically favorable solution is to use the SiC-on-insulator (SiCOI). Akin to SOI, SiCOI structure contains a thin SiC layer isolated by a low-index substrate, so that waveguides and resonators can be patterned on the thin layer to confine light and control its propagation. The first SiCOI for photonics applications made by ion-cutting method were demonstrated by Song et al. [102]. As shown in Figure 4(a), a L3 photonic crystal cavity was fabricated and Q factor of 4500 was measured. Later, 4H-SiCOI was optimized on a wafer-scale, and demonstrated the possibility for mass fabrication by using the CMOS compatible process [103]. The Q value of the microring resonator [104] based on 4H-SiCOI was measured up to 7.3×10^4. The lower Q factor on the ion-cutting SiCOI platform is due to the ion-implantation-induced defects, which dominate the optical absorption loss [104]. Another approach to prepare SiCOI was formed by wafer bonding of crystalline 3C-SiC

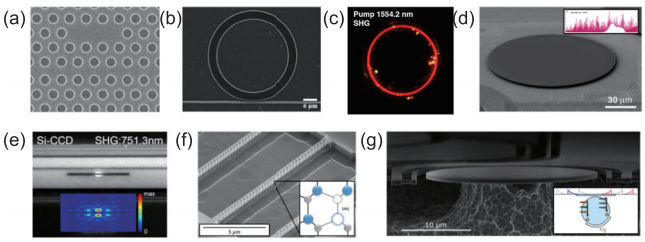

Figure 4 (Color online) SiCOI microresonator. (a) 2D photonic crystal cavity in 6H-SiCOI [102]; (b) microdonut resonators on 3C-SiCOI platform [105]. (c) Microdisk resonator for second-order frequency conversion. The red emission of the image shows the second-harmonic coupled out [98]. (d) Microdisk resonators in 4H-SiCOI. The inset image is the broadband frequency comb spectrum generated from microresonator [98]. (e) The CCD image of the second-harmonic generation under the 1502.58 nm excitation. The inset shows the simulated near-field pattern of the second-harmonic emission [106]. (f) The 4H-SiC photonic crystal nanobeam cavities. The inset is a lattice representation of divacancy defect [99,106]. (g) Waveguide-coupled microdisk resonators in 4H-SiCOI. The inset is the schematic image of Manipulating a pair of emitters implanted in the microdisk [107].

to a silicon oxide-on-Si substrate, which enables high Q of 142000 in 40 μm radius SiC microring resonators [105], as shown in Figure 4(b). However, the Q factor in this platform is still limited by material absorption. In 2019, the grinding and polishing approach was introduced to prepare 4H-SiCOI [95, 106]. In contrast with the previous approaches, this grinding and polishing approach enables 4H-SiC thin films with the same crystalline quality as its pristine crystal, thus high Q microresonators with state-of-the-art reaching the 3-7 million range were achieved [98]. The high Q SiC microresonator stimulates a renewed interest in SiC photonic devices, for example, nonlinear and quantum photonics [107-109].

Figure 4(c) shows a microdisk resonator designed for second-order frequency conversion. The red emission of the image clearly shows the second-harmonic generation [98]. The higher conversion efficiency of 1900% was achieved in a photonic crystal cavity [106], as the photonic crystal cavity shows a smaller modal volume. Such a high conversion efficiency in SiC microresonator holds promises for pumping color center only by telecom wavelength input. Given the record-high Q factors in a SiC microdisk resonator, as shown in Figure 4(d), Wang et al. [98] demonstrated broadband frequency comb generation , which represented a milestone in the development of SiC nonlinear photonic devices. Since SiC hosts a variety of qubits, the SiC microresonator is an ideal platform for a coupled defects zero phonon line (ZPL) emission. Figure 4(f) shows the 4H-SiC photonic crystal nanobeam integrated with a single divacancy color center [99], Purcell enhancement of the ZPL emission with a Purcell factor of ~50 was observed. A clearly increase in the Debye-Waller factor from ~5% to ~70%-75% reveals that the cavity-defect system improves the quantum properties of the color center in SiC. Very recently, the cavity-defect system was used to demonstrate super-radiant emission of the spin emitters [107], as shown in Figure 4(g), this work provides a clear route towards monolithic integration of quantum emitter and nonlinear photonic in 4H-SiCOI.

6 LN

Due to the combination of the excellent photoelectric characteristics of LN crystal and the ability to tightly confine light, LNOI microcavities brings new vitality to LN integrated photonics [110-114]. As a result, they have been a competitive platform for applications ranging from nonlinear frequency conversion and electro-optic modulation, optical frequency combs to laser sources in recent years.

In 2007, the first LNOI microring cavity, as shown in Figure 5(a) [115], was prepared by using benzocyclobutene bonding and photolithographic techniques. Subsequently, the research on the preparation of LNOI microcavity was carried out based on various micro-nano techniques [116-118]. LNOI microcavities (Figure 5(b)) with a quality factor up to 10^7 were obtained by using electron beam exposure-argon ion etching [117] and photolithography-assist-ed chemo-mechanical etching [118], respectively. Thanks to the high nonlinear coefficient of LN, researches on realizing sum-frequency generation (SFG) [119], second-harmonic generation (SHG) [120-124], and cascading second-order nonlinear processes [125] in LNOI microcavity have been reported successively. Among them, to effectively improve the conversion efficiency, Z-cut and X-cut periodically poled lithium niobate (PPLN) microcavities (Figure 5(c)-(e)) were fabricated for the realization of quasi-phase matching [120, 122-124]. In PPLN microcavities, SHG efficiency was optimized up to 52 m W^{-1} [124], which was 3 orders of magnitude higher than monocrystalline LN microcavities [121]. Such an SHG efficiency is also the highest one in all integrated-photonic platforms. Furthermore, spontaneous parametric down-conversion in LNOI microcavities enables the preparation of entangled photon pairs and heralded single-photon sources. A photon-pair generation rate of 36.3 MHz and coincidence-to-accidental ratio of 14682 ± 4427 had been achieved in the LNOI microcavity shown in Figure 5(f) [126].

Micro combs have applications in precision spectroscopy, optical clock, and coherent optical communication due to their compact structure, low noise, and high coherence. Because the rich nonlinear optical characteristics of LN can effectively expand the functionality and application scenarios of micro combs, the research on Kerr micro comb based on LNOI has attracted much attention of researchers. Self-starting soliton micro comb has been realized based on Kerr effect in LNOI microcavity, as shown in Figure 5(g) [127]. Besides, an electro-optic frequency comb based on the LNOI racetrack cavity has also been reported, as shown in Figure 5(h) [128]. Compared with Kerr micro combs, the electro-optical frequency comb has the advantages of no threshold, easy modulation, and low noise.

As an essential part of integrated photonics, laser sources on LNOI platform have also attracted the attention of researchers. Recently, several research groups have successively carried out the research on microcavity lasers based on rare-earth-ions doped LNOI. Erbium-doped and ytterbium-doped microcavity lasers operating at 1550-nm band and 1060-nm band have been demonstrated, respectively [129-132]. In addition, to improve the practicability of the laser, researchers have carried out the research of LNOI single-mode laser through modulation mode loss or Vernier effect [133, 134]. For example, Figure 5(i) shows a single-mode laser with a side-mode suppression ratio of 26.3 dB based on

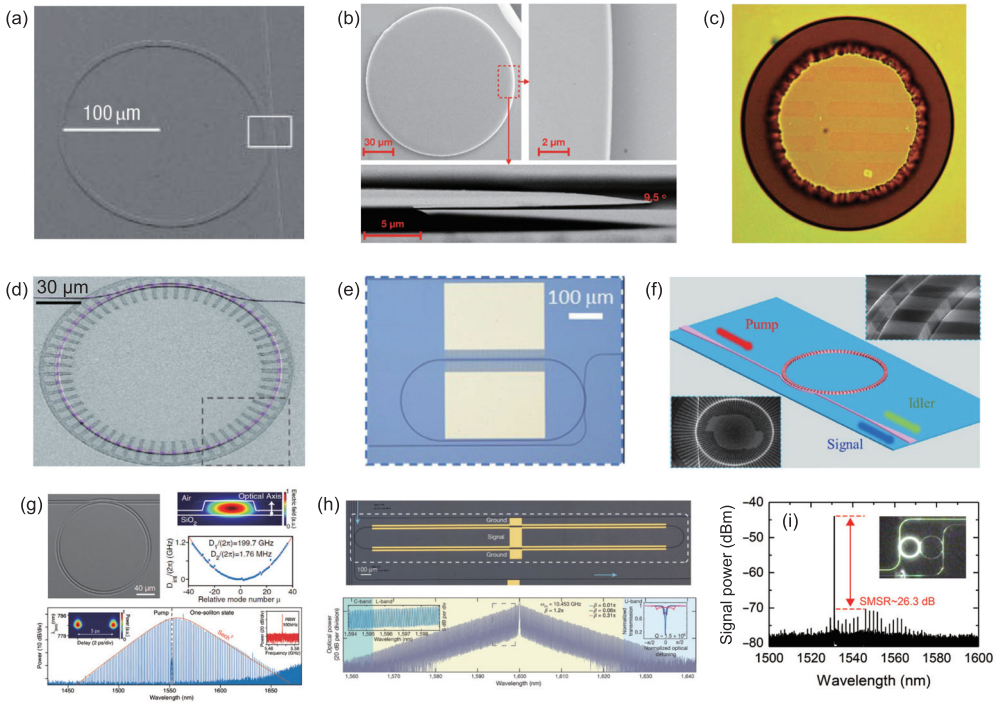

Figure 5 (Color online) Microcavities based on thin-film lithium niobate and its applications. (a) Z-cut microring based on thin-film LN [115]; (b) LNOI microdisk resonator [118]; (c) Z-cut PPLN microdisk [120]; (d) Z-cut PPLN microring [122]; (e) X-cut PPLN microring [123]; (f) sketch and SEM images of LNOI microring for photon-pair generation [126]; (g) self-starting soliton microcomb on Z-cut microring [127]; (h) electro-optic frequency comb on X-cut racetrack microring; (i) single-mode lasers based on LNOI photonic molecule [134].

the Vernier effect [134].

In the future, with the continuous optimization of device preparation and structural design, high-quality LNOI microcavity will become the core part of the integrated photonic chip and play a more critical role in the fields of frequency conversion, light source generation, and on-chip regulation.

7 AlGaAs

AlGaAs and its alloys are among the most widely used III-V semiconductors in integrated photonics for building active devices, such as lasers, modulators and photodetectors. Over the last decade, the value of this group of materials for nonlinear photonics has been discovered and therefore attracted great interests. The most appealing property of AlGaAs is the giant nonlinear effects in both (180 pm/V) and (2.6×10^{-13} cm^2/V) [135], which can significantly enhance the efficiency of nonlinear process. Importantly, by adjusting the material concentrations in the alloys, the bandgap energy can be engineered over broad range (574-872 nm for $Al_xGa_{1-x}As$). As a result, the two photon absorption (TPA) problem can be avoided at telecom bands (1550 and 1310 nm), which is usually a big concern for many III-V materials when performing high power pumping.

To harness these desirable properties for nonlinear applications, one essential requirement is to build the waveguide with high index contrast for flexible geometry engineering. For AlGaAs, previously this was a very challenging task, since the material film has to be grown on native substrate, where the surrounding layers usually have very similar index contrast. To solve this problem, several strategies have been applied over the last two decades. One is to grow the target layer upon aluminum arsenide (AlAs) that is later oxidized to form the aluminum oxid (Al_2O_3) as bottom claddings [136]. This strategy has enabled the demonstration of AlGaAs resonator for optical parametric oscillation [137] and low threshold laser [138]. However, the limitation of these devices is the relative high waveguide loss, which is usually higher than a few dB/cm. Meanwhile, the oxidation process is usually combined with high temperature, which might not be detrimental to the active medium of laser or surface roughness of the waveguide.

Another widely used strategy for building high index-contrast AlGaAs waveguide is to undercut the underneath layer [139, 140], as shown in Figure 6(a)-(c). Similar as the above mentioned structure where the AlGaAs layer sits on AlAs, here the underneath layer is removed by hydrogen fluoride (HF) selectively. The advantage of this approach, compared with the oxidization one, is the room temperature process and the preservation of the surface roughness of the waveguide. As a result, the quality factor of these suspended

whisper-gallery resonators can be significantly improved up to 6×10^6 with the surface passivation treatment [140]. Moreover, since the geometry of waveguide defined by selective etch can be more precisely controlled, the quasi-phase match condition can be satisfied in these resonators, leading to second harmonic generation (SHG) [141].

However, despite the demonstration of individual devices in the last two approaches, the evolving applications in nonlinear photonics demand a more scalable and robust solution to build AlGaAsOI platforms, as shown in Figure 6(d)-(g). Therefore, in last a few years, the heterogeneous integration is introduced to transfer AlGaAs film from native substrate onto oxidized silicon wafer [142-144]. In this way, high-index-contrast, high-material-quality waveguide can be processed in a scalable, repeatable manner [145]. Leveraging advanced lithography, etching and passivation process, high quality microresonator with Q beyond 3.5×10^6 is demonstrated on this platform with much smaller mode volume than those of previous AlGaAsOI waveguide [146]. Such high-Q resonator provides an effective tool to explore the high nonlinearities of AlGaAs alloys: a record low threshold frequency comb generation is enabled in optical frequency generation [143], and a coherent soliton state can be readily achieved under sub-milliwatt pump power [147]; by pumping these microresonator below the threshold, a record high entangled photon generation rate greater than 20×10^9 pairs s^{-1} mW^{-2} has been realized [148]; by using InGaP layer which is lattice-matched to AlGaAs, high quality factor can be achieved at visible, leading to a record high SHG efficiency of 1.5% single photon nonlinearity [149]. Moreover, due to the great advantage in integration level, it is expected that these microresonators will be implemented in PICs along with other photonic components, including lasers, amplifiers, modulators, photoreactors and passives [150].

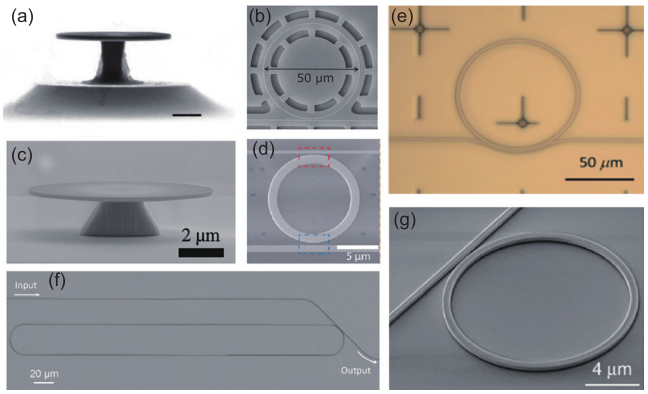

Figure 6 (Color online) AlGaAsOI microresonator. (a)-(c) Suspended AlGaAs structure [139-141]; (d)-(g) AlGaAs/InGaP on SiO_2 [142, 143, 148, 149].

8 Halide perovskite

Halide perovskites, as an emerging class of photovoltaic materials, have attracted considerable attention owing to the outstanding properties, e.g., simple and low-cost synthesis, large optical absorption, long and balanced carrier diffusion length, high carrier mobility, nice defect tolerance, high photoluminescence (PL) quantum yield, and bandgap tunability spanning from visible to near infrared regime [151, 152]. During the past decade, perovskite based devices have undergone substantial progress and become game changer in solar cells [153] and light emitting diodes (LEDs) [154]. Besides, the intrinsic optical merits, including large nonlinearities, relatively high refractive index and high optical gain coefficient, have triggered research interest in perovskite based optical microcavities. Due to the large absorption loss above the material bandgap, perovskites typically function as active photonic devices under optical excitation.

Initial attempt to construct resonant nanostructured perovskite is to integrate perovskite layer with external microcavities by taking advantage of flexible and versatile synthesis methods for perovskites, e.g., spin coating [155], chemical vapor deposition [156] and atomic layer deposition [157]. Later on, direct patterning on perovskite is realized based on the recent development in the modified micro- and nanofabrication techniques, such as focused-ion beam etching, nanoimprinting, laser direct writing. Up to now, diverse resonant structures ranging from microdisk, microring, deformed microcavity, nanograting, to photonic crystal, have been implemented on perovskite and the resonance enhanced device performance confirms the structure-function relation [158].

The highest quality factor of organic-inorganic hybrid perovskite microlasers is achieved by Zhang et al. [159] based on a COMS-compatible manufacturing procedure for perovskite. As shown in Figure 7(a), a circular microdisk with smooth surface is fabricated on a single-crystal perovskite microplate. In addition to circular microdisk, deformed microcavity has also been realized for unidirectional emission (see Figure 7(b)). To address the out-coupling deficiency in circular microdisk, a bus waveguide made of Si_3N_4 or perovskite evanescently coupled to the microdisk has been proposed and demonstrated [160, 161]. Benefiting from the relatively high refractive index, Figure 7(c) shows the perovskite metasurface composed of nanograting for color display [162]. Color variation from different parts, as shown in Figure 7(d), originates from the structure dependent resonant reflection peaks. Furthermore, the perovskite metasurface has been designed to enhance the excitation light resonantly and thereby boosted the three-photon luminescence by a factor of 60 [163]. Based on perovskite mi-

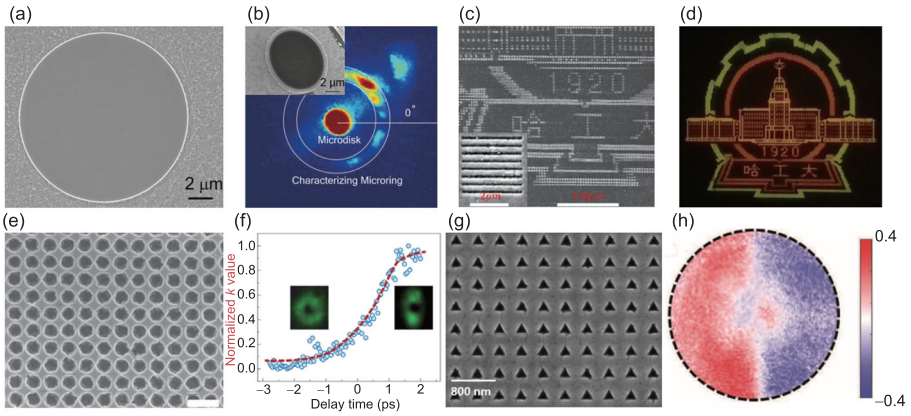

Figure 7 (Color online) Perovskite microcavities and applications. (a), (b) High-quality circular microdisk based on single-crystal perovskite microplate and fluorescence microscope image of a deformed microcavity exhibiting unidirectional emission where inset shows the SEM image [159]. (c), (d) SEM and microscope image of the perovskite metasurface composed of nanograting [162]; (e), (f) SEM image of perovskite photonic crystal and optical switching from vortex beam to linearly polarized beam [164]; (g), (h) SEM image of perovskite metasurface with periodic triangular array and the corresponding degree of circular polarization of PL in the back focal plane [165].

crocavities, Huang et al. [164] have realized vortex microlaser and demonstrated ultrafast all-optical switching. As shown in Figure 7(e), planar photonic crystal with in-plane rotation symmetry is composed of square array of circular holes and affords topologically protected optical bound state in the continuum. By exploiting mode symmetry and far field properties, ultrafast and dynamic optical switching between vortex beam and linearly polarized beam has been achieved (see Figure 7(f)). Interestingly, Tian et al. [165] employed the broken in-plane inversion symmetry to study the optical Rashba effect in monolithic perovskite metasurface, which consists of periodic triangular array as shown in Figure 7(g). Consequently, highly chiral photoluminescence (PL) with six-fold increase in the degree of circular polarization has been demonstrated (see Figure 7(h)), expanding the potential application of perovskite based light-emitting devices to holograph, biosensing and multidimensional multiplexing technologies.

To conclude, resonant microcavities have been widely introduced to perovskite based photovoltaic and optoelectronic devices. The light management involving localization, wave guiding, resonant enhancement and mode conversion in microcavities not only improves the device performance significantly, but also brings novel future applications to perovskites.

9 2D material

Introducing graphene and its derived 2D material into microcavity photonics brings unprecedented opportunities, e.g., broadband optoelectronic tunability and high optical nonlinearity, to engineer the cavity properties for improving the device performances [166-169]. Thanks to their atomically flexible nature, 2D materials are convenient to incorporate into types of microcavity platforms, ranging from on-chip microrings [170], fiber based microresonators [171] and WGM microcavities [172]. In practice, there are a number of strategies for the installation of 2D material-microcavity structures, such as dry transfer, wet transfer and direct vapor/liquid deposition [173-175].

Such implementations diversify the material combinations for microcavity photonics, enabling appealing functions and performances in nanoscale. For instance, by integrating graphene heterostructure in silicon nitride microrings (Figure 8(a)), Phare et al. [176] obtained the spectral shift of resonances can be electrical tuned, thus realized ultrafast electro-optic modulation with 30 GHz bandwidth. Furthermore, in 2018, leveraging the similar geometry, Yao et al. [177] reported that the group velocity dispersion and third-order dispersion intracavity is remarkably gate controllable, from positive to negative. Such a property was successfully applied for delivery diverse Kerr comb outputs in one single device. Recently, via depositing a monolayer of crystalline Mo_3Te_4 in a 1-THz free spectral range (FSR) Si_3N_4 microcavity, He et al. [178] achieved a quality factors more than 3×10^6 in the O to E bands, and demonstrated that such a 2D material enhanced microcavity can have third order nonlinear susceptibility $\chi^{(3)} = 10^{-18}$-10^{-15}, potential to ultralow threshold frequency conversion applications.

Figure 8(b) illustrates several examples. Related to on-chip microrings, the material-incorporation in WGM microcavities is simpler, in which cladding-etching is not in-need. By inner-depositing pr-GO in microfluidic cavities, Brillouin opto-mechnical oscillation and fluorescence resonance energy transfer (FRET) were observed, and applied in ultrasen-

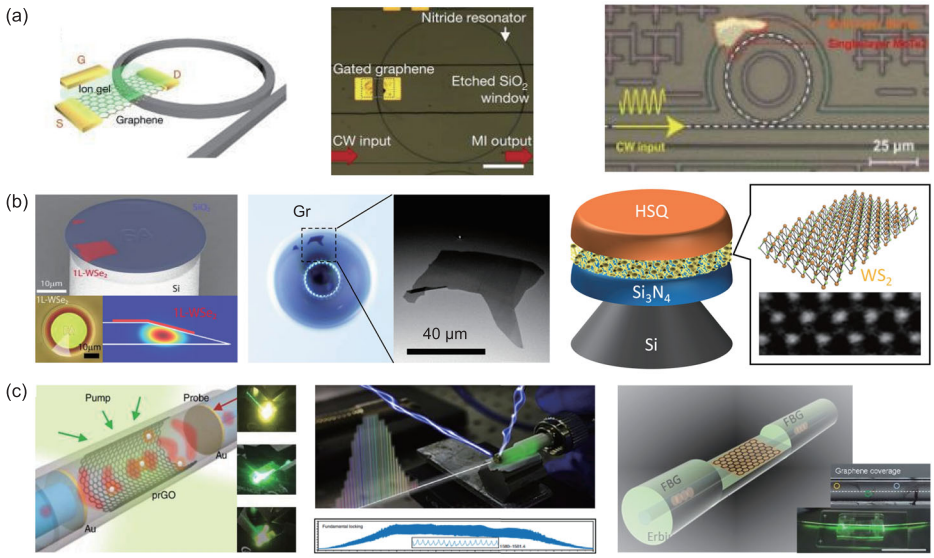

Figure 8 (Color online) 2D material based microresonators. (a) 2D material deposited in silicon based microrings on-chip, from left to right: [177, 178]. (b) 2D material incorporated WGM microcavities, from left to right: [181, 182]. (c) 2D material functionalized fiber microresonators, from left to right: [180, 186, 187].

sitive biochemical tracing [179, 180]. In a silica microdisk, Javerzac-Galy et al. [181] demonstrated that excitonic emission is achieved by in the evanescent oscillation; Tan et al. [182] deposited graphene monolayer in an over-modal silica microsphere, enabling modal-selective control of Stokes solitons, thus enabled multi-channel detections in radio frequency band. Recently, researches also shew that the 2D material with a bandgap (e.g., Tungsten Disulfide (WS_2)), can be macroscopically configured via lithography to be the core of a microcavity, serving as the gain material and realize lasing excitation [183, 184].

Besides the aforementioned two geometries, in 2D material can also functionalize fiber microcavities, when covering on the end or side face of a fiber section intracavity (Figure 8(c)). In a graphene bipolar-junction integrated Fabry-Perot fiber microcavity with 10 GHz repetition, Martinez and Yamashita [185] reported the first passive mode-locked laser in millimeter scale. Beyond that, Qin et al. [186] demonstrated electrically dynamical control and active feedback of laser frequency combs, with 2f-3f span and fully-suppressed phase noise down to −120 dBc/Hz@10 kHz. By covering graphene in a D-shape fiber based Distributed Bragg Mirror (DBR) microlaser cavity with repetition 2.5 GHz, Guo et al. [187] realized the Q-switching cavity-oscillation dual mode excitation, these two modes are independently sensitive to external alteration, enabling dual-species gas detection in mixture. With the development of large-scale industrial preparation of 2D materials, it is expectable that 2D material based microresonators are going towards to wide practical potentials in devices and systems out of lab.

10 Organic molecules

Organic molecules with extended π-electron conjugation can have large electric dipole elements for optical transition. The nonlinear optical responses of organic molecules are dominated by their electronic states, making their off-resonant response instantaneously. The strong electronic nonlinearities and fast optical response of organic materials, make them very attractive as active materials to incorporate into various integrated optical configurations for advanced photonic applications [188]. For instance, organic-hybrid, chip-scale silicon slot waveguides and photonic crystal microcavities have made great progress in high speed electro-optic modulations [189, 190] and all-optical signal processing [191-193] over two decades. Recently, nonlinear optical molecules were adapted to hybrid with ultra-high Q microcavity devices, bringing new opportunities to enable novel functionalities and enhanced performance for nonlinear photonics [194, 195].

Strategies to incorporate organic materials into photonics platforms are flexible for different purposes (Figure 9). Organic molecules doped in polymers can be easily spin-coated on various photonic substrates to form the desired dense solid state assembles [196, 197] (Figure 9(a) and (b)). Polymers can also be direct-casted on the surface of whispering gallery mode microcavities (Figure 9(c)), or lithographed from thin films on silicon substrates to form high Q hybrid devices [198-200] (Figure 9(d)). Recently, a very low-loss, chemical vapor deposition method is utilized to covalently incorporate single nanolayers of organic molecules on silica mi-

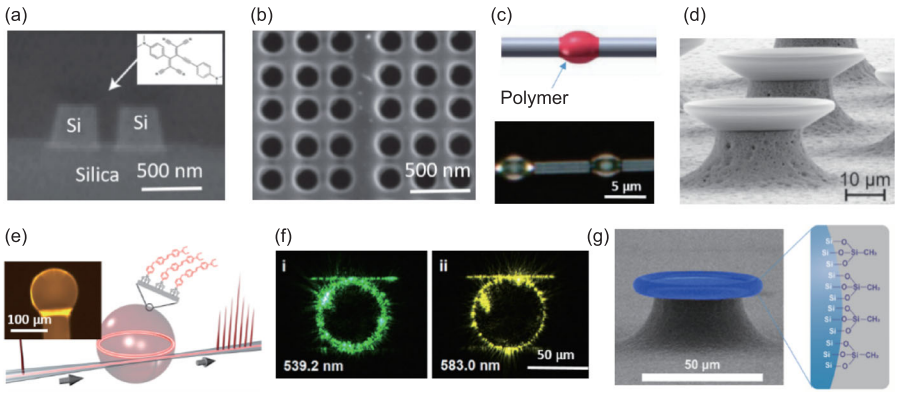

Figure 9 (Color online) Organic-hybrid microcavities. (a) An organic-hybrid silicon-on-insulator device fabricated by physical vapor deposition [191]; (b) a hybrid two dimensional photonic cavity filled with an organic dye-doped polymer [192]; (c) a polymer microbottle resonator by directly drop-casting a polymer solution on a silica fiber [198]; (d) on-chip conical polymer microresonators by direct lithographing polymethyl methacrylate (PMMA) film on silicon substrate [200]. (e) Schematic on an ultrahigh Q organic-hybrid microsphere for frequency comb generation [194]. The microsphere is grated with a smooth single layer of molecules via chemical vapor deposition. Inset is a fluorescent image of a hybrid microsphere. (f) Bright multi-color images of third-order harmonic emissions from an ultrahigh Q organic-hybrid microsphere [195]; (g) an on-chip ultrahigh Q toroidal microresonator grafted with a self-constrained single molecular layer for surface Raman lasing [203].

crosonators [194, 201]. Thanks to the precision of the monolayer formation, ultrahigh Q values of above 5×10^7 were achieved. The ultrahigh Q organic-hybrid techniques have great potential to enable radically new devices which can boost the efficiencies of various nonlinear processes dramatically [202].

For examples, Shen et al. [194] successfully demonstrated an organic molecule-driven strategy to generate low-threshopd frequency combs in ultrahigh Q organic-hybrid microcavities (Figure 9(e)). An organic nonlinear optical molecule named 4-[4-diethylamino(styryl)] pyridinium (DSP) was grafted on the surface of a silica spherical microcavity to form a single molecular layer. The large Kerr coefficient of the surface molecular layer significantly increases the overall Kerr nonlinearity of the hybrid microcavity, which subsequently help suppress the common, parasitic Raman effect. The effective parametric gain bandwidth of the hybrid microsphere was approximately one order of magnitude larger than silica microsphere, leading to leading an efficiency improvement of three orders of magnitude in optical parametric oscillation. By further leveraging the third-order nonlinearities of the organic layer, the organic-hybrid microcavity was studied for enhanced third harmonic generation (THG) through dynamic phase matching [195]. A record conversion efficiency of $\sim 1680\%/\mathrm{W}^2$ was achieved for THG, which is about four-order of magnitude higher compared with a nonfunctional silica microcavity. As shown in (Figure 9(f)), bright multi-color images of third-order harmonic and sum frequency emissions from an ultrahigh Q organic-hybrid microsphere. More recently, by using ultrahigh Q organic-hybrid techniques, Shen et al. [203] demonstrated a distinct nonlinear Raman behavior called surface stimulated Raman scattering (SSRS) on an integrated photonic device. By creating a self-constrained, oriented siloxane monolayer on the surface of integrated toroidal microresonators (Figure 9(g)), the TE/TM dependent SSRS was observed with low threshold powers (200 μW). Owing to the ordered organic monolayer, improvement in the Raman lasing efficiency from 5% to 40% was demonstrated.

While the high Q organic hybrid techniques have showed immediate impact on nonlinear optics, it is still in the infant stage. So far, most of the demonstrated microcavity nonlinear behaviors are based on third-order nonlinearities of molecules. It would be of great promise to further leverage the large second-order hyperpolarizabilities of asymmetric organic molecules to enable the generation of on-chip second-order nonlinear frequency conversions, such as second-order harmonic generation, three-wave mixing and oscillation, and Pockels frequency combs. Optical or electrical modulation of microcombs could also be enabled via controlling the surface organic molecules. Benefiting from the large optical nonlinearities and rich chemical and physical functionalities, ultrahigh Q organic-hybrid microcavities would have bright future in integrated photonics, for not only enhanced efficiencies but also novel functions.

11 Diamond membrane

Advancement of diamond based photonic circuitry requires robust fabrication protocols of key components including diamond resonators and cavities [204-206]. The advent of commercially available, high-quality single crystal diamonds boosted a decade of research rendering diamond as one of

the most studied platforms for novel quantum technologies [207]. The availability of diamond colour centres (e.g., nitrogen [208] silicon [209], or germanium [210-215] vacancies) that can be utilised as solid state qubits motivated the advance of diamond nanofabrication processes.

For many applications, including integration with fibre cavities [216-219] and on chip devices [220-222], planar geometries are required to satisfy the requirement of optical isolation of the diamond device through refractive index contrast while minimising the size of the diamond components, which is challenging with bulk diamond fabrication methods. Of particular interest is engineering of thin diamond membranes and consequently photonic resonators including PCC, microrings and waveguides [212, 215, 217, 222-228], Figure 10(a) demonstrates such a diamond membrane, with characteristic SiV and GeV emission. These devices are needed for both integrated diamond photonics on a single chip, and an improved collection efficiency of photons emitted from the embedded emitters [229-234].

Figure 10(c) and (d) show one such example of a 128-channel photonic integrated artificial atom chip containing diamond quantum emitters with high coupling efficiencies, optical coherences near the lifetime limit and tuneable optical frequencies to compensate for spectral inhomogeneities on chip [235]. Coupling the emitters to photonic crystal cavities also constitutes the realisation of a Purcell enhancement that is needed to enhance the emission rate of photons into the zero photon line (ZPL), thus achieving a coherent photon emission [236-239]. Examples of membrane-based structures are demonstrated in Figure 10(e) and (f), showing a nanobeam cavity and photonic crystal cavity respectively. Figure 10(g) demonstrates a manual transferring technique which has been demonstrated allowing the transfer of fabricated diamond membrane cavities between substrates, allowing photonic components to be generates as modular components for wider photonic circuitry as in Figure 10(c) and (d). In extension to this capability, the lack of fabrication constraints and imposition of triangular cross section often seen in bulk undercutting techniques allow membranes to act as ideal candidates for advanced designs for photonic cavities. Figure 10(h) demonstrates an inverse design technique resulting in a vertical coupling nodule at the end of a membrane based suspended waveguide, the red colourisation indicating the field intensities in the z direction [240]. Figure 10(i) shows the optimisation of structure as it approaches a fabrication limited structure.

Several nanofabrication approaches to create photonic cavities from diamond membranes have been established which cater to challenges in thin film fabrication [241-248]. Of these, notably the use of transferrable hard masks, fabricated from silicon materials, have been employed as making materials, utilising the superior fabrication processing power of the silicon industry to bare on diamond [249]. HSQ masking is one of the more common patterning and etching techniques, taking advantage of the opposing dry etch chemistries of diamond and silicon dioxide to achieve high selectivity under oxygen plasma etching along side the convenience of direct write masking [212, 215, 228, 250]. Metal masking, including tungsten, has been shown to address the need for reliable nanoscale masking for the generation of feature sizes

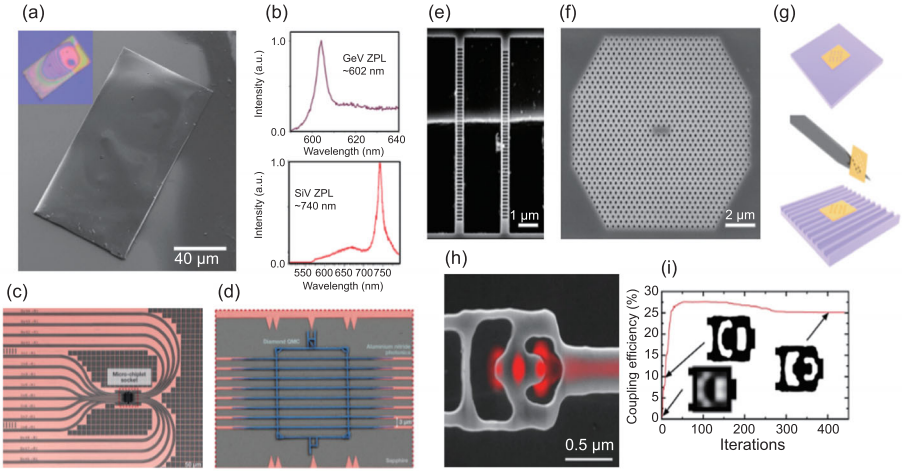

Figure 10 (Color online) Sub micron single crystal diamond membranes and their applications. (a) SEM image of diamond membrane with inset optical image; (b) characteristic spectrum of SiV and GeV emission from. (c) An AlN-on-sapphire integrated photonics module that interfaces with the diamond quantum microchiplet placed in the chiplet socket [235]. (d) Close-up SEM of the diamond quantum microchiplet and AlN photonic interfaces. SEM image of membrane fabricated (e) nanobeam cavity and (f) photonic crystal cavity [247]. (g) Representation of transfer process of fabricated cavities [247]; (h) SEM image of inverse-designed vertical coupler with simulated fields superimposed in red. (i) In-coupling efficiency during design optimization; insets illustrate different optimization phases. The small performance drop beyond 200 iterations of optimization occurs when fabrication constraints are imposed [240].

Table 1 List of key properties of some commonly used materials in photonics

Material	Optical refractive index	Bandgap (eV)	Second-order nonlinear coefficient (pm/V)	Nonlinear refractive index, n_2 (m^2/W)	Quality factor (million)
Doped silica	1.44 [50]	0	0	2.2×10^{-20} @1550 nm [135]	270 [23]
SiN	1.98 [50]	5 [50]	0	2.5×10^{-19} @1550 nm [135]	30 [62]
AlN	2.12(o) [77]	6.2 [77]	d_{33} = 4.7 @1550 nm [77]	2.3×10^{-19} @1550 nm [76]	1 [78]
SiC	2.6 [93]	3.26 for 4H polytype [93]	d_{33} = 30 @1550 nm [93]	10^{-18} @1550 nm [93]	7 [93]
LN	2.2(o) [110]	3.11 [111]	d_{33} = 27 @1064 nm [110]	1.8×10^{-19} @1550 nm [110]	50 [112]
AlGaAs	3.3 [93]	1.63 [93]	d_{36} = 180 @1550 nm [135]	2.6×10^{-17} @1550 nm [135]	6 [140]
Halide perovskite (such as $MAPbX_3$)	~1.9 (X=Br) [163]	2.32 (X=Br) [163]	0	8.36×10^{-15} @1064 nm (X = Cl) [151]	0.01 [73]
2D material (such as $1L-MoTe_2$)	~2.8 @730 [168]	1.1 [178]	0	~ 10^{-15} @1550 nm [178]	3 [178]
Organic molecules (such as DASP molecules)	1.8 [204]	1.77 [204]	d_{33} = 12400 @1064 nm [205]	2.54×10^{-17} @1550 nm [195]	24 [195]
Diamond	2.4 [206]	5.5 [206]	0	8.2×10^{-20} @1550 nm [206]	1 [206]

on membranes at the scale requires of photonic components [247]. The development of robust diamond fabrication techniques pave to way toward realisation of diamond based photonic circuitry and modular photonic components.

12 Outlook

Recent developments of new material platforms for chip-based microcavities have radically impacted the ways in which we tailor the light-matter interactions in nanoscale. We have witnessed a whole new generation of microcavity devices with unprecedented performances and expanded functionalities. Table 1 presents an overview for the material parameters and typical Q factors of the optical microresonators made from the integrated material platforms discussed in this review. Despite of the variation of the material properties in terms of the refractive index, bandgap, and optical nonlinearity, Q factors above 1 million are reproducible achievable in all of the planar microresonators. In particular, microcavties with Q-factors up to a few tens of million can be readily fabricated in a whole wafer thanks to the development of the ultra-low loss SiN material and its fabrication process [62]. The turnkey performance of microcomb soliton devices could immediately and commercial applications such as LiDARs in self-driving cars [251]. The SiN and doped silica appear to be very promising for the emerging applications based on the microcomb technology. III-V compound materials, such as AlGaAs are more favorable when direct bandgap is required for light emission processes. LN currently exhibits superior device performances as ultra-fast modulators with low-power consumption. In the quantum regime, the spin states in the defects of SiC and diamond could serve as spin-photon interfaces for future quantum networks. However, it is extremely challenging for any one of these material platforms to meet the stringent demands for all the applications simultaneously. Hybrid platforms that combine different photonic materials on a single chip provide a viable path to overcome the limitations of single material systems. One of the representative examples is to fast actuate soliton microcomb in SiN by using integrated piezoelectric components made of AlN [251]. Yet, the design and fabrication of hybrid integrated microcavities are at large a very challenging engineering task. There are a variety of heterogeneous integration methods including heteroepitaxy, wafer bonding, transfer-print. These techniques have been demonstrated to be very successful for the heterogeneous integration for some of the materials we discussed in this review. Yet, it is still challenging to build hybrid material platforms that combine very specific materials with very different properties. In addition, the pursuit of the new generation of photonic functional devices usually requests optical materials with extreme properties, e.g., transparent ferroelectric crystals with ultrahigh piezoelectricity [252], which keeps on driving the community to explore new material platforms, and novel fabrication processes. Moving forward, both developments in new material platforms and hybrid integration of existing systems are crucial for advancing the microcavity devices in the future.

This work was supported by the National Natural Science Foundation of China (Grant Nos. 61234003, 61434004, and 61504141), National Key Research and Development Program of China, and CAS Interdisciplinary Project (Grant No. KJZD-EW-L11-04).

1 K. J. Vahala, Nature **424**, 839 (2003).
2 J. Ward, and O. Benson, Laser Photon. Rev. **5**, 553 (2011).
3 S. Feng, T. Lei, H. Chen, H. Cai, X. Luo, and A. W. Poon, Laser

Photon. Rev. **6**, 145 (2012).
4 Q. H. Song, Sci. China-Phys. Mech. Astron. **62**, 074231 (2019).
5 P. W. Higgs, Phys. Rev. Lett. **13**, 508 (1964).
6 F. Englert, and R. Brout, Phys. Rev. Lett. **13**, 321 (1964).
7 A. Altland, and B. D. Simons, *Condensed Matter Field Theory* (Cambridge University Press, Cambridge, 2010).
8 Q. T. Cao, H. Wang, C. H. Dong, H. Jing, R. S. Liu, X. Chen, L. Ge, Q. Gong, and Y. F. Xiao, Phys. Rev. Lett. **118**, 033901 (2017), arXiv: 1607.01459.
9 O. Painter, R. K. Lee, A. Scherer, A. Yariv, J. D. O'Brien, P. D. Dapkus, and I. Kim, Science **284**, 1819 (1999).
10 R. F. Oulton, V. J. Sorger, T. Zentgraf, R. M. Ma, C. Gladden, L. Dai, G. Bartal, and X. Zhang, Nature **461**, 629 (2009).
11 D. Liang, and J. E. Bowers, Nat. Photon. **4**, 511 (2010).
12 L. He, Ş. K. Özdemir, and L. Yang, Laser Photon. Rev. **7**, 60 (2013).
13 H. Rong, A. Liu, R. Jones, O. Cohen, D. Hak, R. Nicolaescu, A. Fang, and M. Paniccia, Nature **433**, 292 (2005).
14 H. Rong, R. Jones, A. Liu, O. Cohen, D. Hak, A. Fang, and M. Paniccia, Nature **433**, 725 (2005).
15 Y. Takahashi, Y. Inui, M. Chihara, T. Asano, R. Terawaki, and S. Noda, Nature **498**, 470 (2013).
16 Q. Xu, B. Schmidt, S. Pradhan, and M. Lipson, Nature **435**, 325 (2005).
17 J. T. Robinson, L. Chen, and M. Lipson, Opt. Express **16**, 4296 (2018).
18 M. R. Lee, and P. M. Fauchet, Opt. Express **15**, 4530 (2007).
19 E. Luan, H. Shoman, D. M. Ratner, K. C. Cheung, and L. Chrostowski, Sensors **18**, 3519 (2018).
20 S. Chu, and B. Little, in *High-index doped silica glass planar lightwave circuits: Proceedings of the OSA Advanced Photonics Congress 2021* (Optica Publishing Group, Washington, 2021).
21 B. E. Little, and S. T. Chu, Opt. Photon. News **11**, 24 (2000).
22 D. J. Moss, R. Morandotti, A. L. Gaeta, and M. Lipson, Nat. Photon. **7**, 597 (2013), arXiv: 1404.3775.
23 J. Li, H. Lee, T. Chen, and K. J. Vahala, Phys. Rev. Lett. **109**, 233901 (2012), arXiv: 1208.5256.
24 B. E. Little, S. T. Chu, P. P. Absil, J. V. Hryniewicz, F. G. Johnson, F. Seiferth, D. Gill, V. van, O. King, and M. Trakalo, IEEE Photon. Technol. Lett. **16**, 2263 (2004).
25 D. Duchesne, M. Peccianti, M. R. E. Lamont, M. Ferrera, L. Razzari, F. Légaré, R. Morandotti, S. Chu, B. E. Little, and D. J. Moss, Opt. Express **18**, 923 (2010).
26 M. Peccianti, M. Ferrera, L. Razzari, R. Morandotti, B. E. Little, S. T. Chu, and D. J. Moss, Opt. Express **18**, 7625 (2010).
27 A. Kovach, D. Chen, J. He, H. Choi, A. H. Dogan, M. Ghasemkhani, H. Taheri, and A. M. Armani, Adv. Opt. Photon. **12**, 135 (2020), arXiv: 2001.00650.
28 Y. Xu, Y. Yang, X. Li, X. Wang, and W. Zou, Chin. Opt. Lett. **19**, 113902 (2021).
29 L. Razzari, D. Duchesne, M. Ferrera, R. Morandotti, S. Chu, B. E. Little, and D. J. Moss, Nat. Photon. **4**, 41 (2010).
30 A. Pasquazi, R. Ahmad, M. Rochette, M. Lamont, B. E. Little, S. T. Chu, R. Morandotti, and D. J. Moss, Opt. Express **18**, 3858 (2010), arXiv: 1705.00778.
31 M. Kues, C. Reimer, B. Wetzel, P. Roztocki, B. E. Little, S. T. Chu, T. Hansson, E. A. Viktorov, D. J. Moss, and R. Morandotti, Nat. Photon. **11**, 159 (2017).
32 Y. Li, S. H. Wang, Y. Tian, W. L. Ho, Y. Li, L. Wang, R. R. Davidson, B. E. Little, and S. T. Chu, Opt. Express **28**, 641 (2020).
33 Z. Lu, W. Wang, W. Zhang, M. Liu, L. Wang, S. T. Chu, B. E. Little, J. Zhao, P. Xie, X. Wang, and W. Zhao, Opt. Mater. Express **8**, 2662 (2018).
34 W. Wang, Z. Lu, W. Zhang, S. T. Chu, B. E. Little, L. Wang, X. Xie, M. Liu, Q. Yang, L. Wang, J. Zhao, G. Wang, Q. Sun, Y. Liu, Y. Wang, and W. Zhao, Opt. Lett. **43**, 2002 (2018).
35 W. Wang, L. Wang, and W. Zhang, Adv. Photon. **2**, 1 (2020).
36 X. Wang, P. Xie, W. Wang, Y. Wang, Z. Lu, L. Wang, S. T. Chu, B. E. Little, W. Zhao, and W. Zhang, Photon. Res. **9**, 66 (2021).
37 X. Wang, P. Xie, W. Wang, Y. Wang, Z. Lu, L. Wang, S. T. Chu, B. E. Little, W. Zhao, and W. Zhang, Photon. Res. **9**, 66 (2021).
38 W. Wang, W. Zhang, Z. Lu, S. T. Chu, B. E. Little, Q. Yang, L. Wang, and W. Zhao, Photon. Res. **6**, 363 (2018).
39 Y. Zhao, L. Chen, C. Zhang, W. Wang, H. Hu, R. Wang, X. Wang, S. T. Chu, B. Little, W. Zhang, and X. Zhang, Laser Photon. Rev. **15**, 2100264 (2021).
40 Y. Zhao, L. Chen, W. Wang, R. Wang, H. Hu, X. Wang, C. Zhang, W. Zhang, and X. Zhang, APL Photon. **5**, 046102 (2020).
41 Z. Lu, H. J. Chen, W. Wang, L. Yao, Y. Wang, Y. Yu, B. E. Little, S. T. Chu, Q. Gong, W. Zhao, X. Yi, Y. F. Xiao, and W. Zhang, Nat. Commun. **12**, 3179 (2021).
42 T. G. Nguyen, M. Shoeiby, S. T. Chu, B. E. Little, R. Morandotti, A. Mitchell, and D. J. Moss, Opt. Express **23**, 22087 (2015), arXiv: 1512.01741.
43 X. Xu, M. Tan, J. Wu, T. G. Nguyen, S. T. Chu, B. E. Little, R. Morandotti, A. Mitchell, and D. J. Moss, J. Lightwave Technol. **37**, 1288 (2019), arXiv: 1903.08541.
44 M. Tan, X. Xu, A. Boes, B. Corcoran, J. Wu, T. G. Nguyen, S. T. Chu, B. E. Little, R. Morandotti, A. Mitchell, and D. J. Moss, J. Lightwave Technol. **38**, 6221 (2020).
45 J. Wang, Z. Lu, W. Wang, F. Zhang, J. Chen, Y. Wang, J. Zheng, S. T. Chu, W. Zhao, B. E. Little, X. Qu, and W. Zhang, Photon. Res. **8**, 1964 (2020).
46 B. Corcoran, M. Tan, X. Xu, A. Boes, J. Wu, T. G. Nguyen, S. T. Chu, B. E. Little, R. Morandotti, A. Mitchell, and D. J. Moss, Nat. Commun. **11**, 2568 (2020).
47 F. X. Wang, W. Wang, R. Niu, X. Wang, C. L. Zou, C. H. Dong, B. E. Little, S. T. Chu, H. Liu, P. Hao, S. Liu, S. Wang, Z. Q. Yin, D. Y. He, W. Zhang, W. Zhao, Z. F. Han, G. C. Guo, and W. Chen, Laser Photon. Rev. **14**, 1900190 (2020), arXiv: 1812.11415.
48 M. Kues, C. Reimer, J. M. Lukens, W. J. Munro, A. M. Weiner, D. J. Moss, and R. Morandotti, Nat. Photon. **13**, 170 (2019), arXiv: 2001.02356.
49 X. Xu, M. Tan, B. Corcoran, J. Wu, A. Boes, T. G. Nguyen, S. T. Chu, B. E. Little, D. G. Hicks, R. Morandotti, A. Mitchell, and D. J. Moss, Nature **589**, 44 (2021), arXiv: 2011.07393.
50 C. G. H. Roeloffzen, M. Hoekman, E. J. Klein, L. S. Wevers, R. B. Timens, D. Marchenko, D. Geskus, R. Dekker, A. Alippi, R. Grootjans, A. van Rees, R. M. Oldenbeuving, J. P. Epping, R. G. Heideman, K. Worhoff, A. Leinse, D. Geuzebroek, E. Schreuder, P. W. L. van Dijk, I. Visscher, C. Taddei, Y. Fan, C. Taballione, Y. Liu, D. Marpaung, L. Zhuang, M. Benelajla, and K. J. Boller, IEEE J. Sel. Top. Quantum Electron. **24**, 1 (2018).
51 T. J. Kippenberg, A. L. Gaeta, M. Lipson, and M. L. Gorodetsky, Science **361**, 567 (2018).
52 S. Wan, R. Niu, J. L. Peng, J. Li, G. C. Guo, C. L. Zou, and C. H. Dong, Chin. Opt. Lett. **20**, 032201 (2022).
53 H. Zhou, Y. Geng, W. Cui, S. W. Huang, Q. Zhou, K. Qiu, and C. W. Wong, Light Sci. Appl. **8**, 50 (2019).
54 M. Shen, K. Yin, R. Miao, Z. Xu, J. Yang, X. Zheng, and T. Jiang, in *G eneration of a 100 GHz Kerr soliton frequency comb in an auxiliary laser assisted Si_3N_4 micro-ring resonator: Proceedings of the Twelfth International Conference on Information Optics and Photonics* (SPIE, Xi'an, 2021), Vol. 12057, pp. 843-846.
55 V. Brasch, M. Geiselmann, T. Herr, G. Lihachev, M. H. P. Pfeiffer, M. L. Gorodetsky, and T. J. Kippenberg, Science **351**, 357 (2015).
56 M. Yu, J. K. Jang, Y. Okawachi, A. G. Griffith, K. Luke, S. A. Miller, X. Ji, M. Lipson, and A. L. Gaeta, Nat. Commun. **8**, 14569 (2017), arXiv: 1609.01760.
57 S. Wan, R. Niu, Z. Y. Wang, J. L. Peng, M. Li, J. Li, G. C. Guo, C. L. Zou, and C. H. Dong, Photon. Res. **8**, 1342 (2020).
58 M. Karpov, M. H. P. Pfeiffer, H. Guo, W. Weng, J. Liu, and T. J. Kippenberg, Nat. Phys. **15**, 1071 (2019), arXiv: 1903.07122.
59 Z. L. Newman, V. Maurice, T. Drake, J. R. Stone, T. C. Briles, D. T. Spencer, C. Fredrick, Q. Li, D. Westly, B. R. Ilic, B. Shen, M. G.

Suh, K. Y. Yang, C. Johnson, D. M. S. Johnson, L. Hollberg, K. J. Vahala, K. Srinivasan, S. A. Diddams, J. Kitching, S. B. Papp, and M. T. Hummon, Optica **6**, 680 (2019).
60 J. Riemensberger, A. Lukashchuk, M. Karpov, W. Weng, E. Lucas, J. Liu, and T. J. Kippenberg, Nature **581**, 164 (2020), arXiv: 1912.11374.
61 J. Liu, E. Lucas, A. S. Raja, J. He, J. Riemensberger, R. N. Wang, M. Karpov, H. Guo, R. Bouchand, and T. J. Kippenberg, Nat. Photon. **14**, 486 (2020).
62 J. Liu, G. Huang, R. N. Wang, J. He, A. S. Raja, T. Liu, N. J. Engelsen, and T. J. Kippenberg, Nat. Commun. **12**, 2236 (2021), arXiv: 2005.13949.
63 B. Shen, L. Chang, J. Liu, H. Wang, Q. F. Yang, C. Xiang, R. N. Wang, J. He, T. Liu, W. Xie, J. Guo, D. Kinghorn, L. Wu, Q. X. Ji, T. J. Kippenberg, K. Vahala, and J. E. Bowers, Nature **582**, 365 (2020).
64 C. Xiang, J. Liu, J. Guo, L. Chang, R. N. Wang, W. Weng, J. Peters, W. Xie, Z. Zhang, J. Riemensberger, J. Selvidge, T. J. Kippenberg, and J. E. Bowers, Science **373**, 99 (2021).
65 Z. Ye, P. Zhao, K. Twayana, M. Karlsson, V. Torres-Company, and P. A. Andrekson, Sci. Adv. **7**, eabi8150 (2021).
66 H. Guo, C. Herkommer, A. Billat, D. Grassani, C. Zhang, M. H. P. Pfeiffer, W. Weng, C. S. Brès, and T. J. Kippenberg, Nat. Photon. **12**, 330 (2018).
67 Y. Okawachi, B. Y. Kim, Y. Zhao, X. Ji, M. Lipson, and A. L. Gaeta, Optica **8**, 1458 (2021).
68 Y. Zhang, M. Menotti, K. Tan, V. D. Vaidya, D. H. Mahler, L. G. Helt, L. Zatti, M. Liscidini, B. Morrison, and Z. Vernon, Nat. Commun. **12**, 2233 (2021), arXiv: 2001.09474.
69 W. Jin, Q. F. Yang, L. Chang, B. Shen, H. Wang, M. A. Leal, L. Wu, M. Gao, A. Feshali, M. Paniccia, K. J. Vahala, and J. E. Bowers, Nat. Photon. **15**, 346 (2021), arXiv: 2009.07390.
70 X. Ji, X. Yao, Y. Gan, A. Mohanty, M. A. Tadayon, C. P. Hendon, and M. Lipson, APL Photon. **4**, 090803 (2019).
71 A. Rao, G. Moille, X. Lu, D. A. Westly, D. Sacchetto, M. Geiselmann, M. Zervas, S. B. Papp, J. Bowers, and K. Srinivasan, Light Sci. Appl. **10**, 109 (2021), arXiv: 2010.09479.
72 G. Liang, H. Huang, A. Mohanty, M. C. Shin, X. Ji, M. J. Carter, S. Shrestha, M. Lipson, and N. Yu, Nat. Photon. **15**, 908 (2021).
73 Z. He, B. Chen, Y. Hua, Z. Liu, Y. Wei, S. Liu, A. Hu, X. Shen, Y. Zhang, Y. Gao, and J. Liu, Adv. Opt. Mater. **8**, 2000453 (2020).
74 H. Tian, J. Liu, A. Siddharth, R. N. Wang, T. Blésin, J. He, T. J. Kippenberg, and S. A. Bhave, Nat. Photon. **15**, 828 (2021), arXiv: 2104.01158.
75 Z. Wu, T. Zhang, Y. Chen, Y. Zhang, and S. Yu, Phys. Status Solidi RRL **13**, 1800338 (2019).
76 H. Jung, C. Xiong, K. Y. Fong, X. Zhang, and H. X. Tang, Opt. Lett. **38**, 2810 (2013).
77 C. Xiong, W. H. P. Pernice, X. Sun, C. Schuck, K. Y. Fong, and H. X. Tang, New J. Phys. **14**, 095014 (2012), arXiv: 1210.0975.
78 X. Guo, C. L. Zou, and H. X. Tang, Optica **3**, 1126 (2016).
79 A. W. Bruch, X. Liu, J. B. Surya, C. L. Zou, and H. X. Tang, Optica **6**, 1361 (2019), arXiv: 1909.07422.
80 J. Q. Wang, Y. H. Yang, M. Li, X. X. Hu, J. B. Surya, X. B. Xu, C. H. Dong, G. C. Guo, H. X. Tang, and C. L. Zou, Phys. Rev. Lett. **126**, 133601 (2021), arXiv: 2011.10352.
81 X. Liu, Z. Gong, A. W. Bruch, J. B. Surya, J. Lu, and H. X. Tang, Nat. Commun. **12**, 5428 (2021), arXiv: 2012.13496.
82 H. Weng, A. A. Afridi, J. Liu, J. Li, J. Dai, X. Ma, Y. Zhang, Q. Lu, W. Guo, and J. F. Donegan, Opt. Lett. **46**, 3436 (2021), arXiv: 2102.10311.
83 L. Fan, C. L. Zou, R. Cheng, X. Guo, X. Han, Z. Gong, S. Wang, and H. X. Tang, Sci. Adv. **4**, eaar4994 (2018), arXiv: 1805.04509.
84 Z. Shen, X. Han, C. L. Zou, and H. X. Tang, Rev. Sci. Instrum. **88**, 123709 (2017), arXiv: 1712.01273.
85 X. Liu, C. Sun, B. Xiong, L. Wang, J. Wang, Y. Han, Z. Hao, H. Li, Y. Luo, J. Yan, T. Wei, Y. Zhang, and J. Wang, Optica **4**, 893 (2017).
86 A. W. Bruch, X. Liu, Z. Gong, J. B. Surya, M. Li, C. L. Zou, and H. X. Tang, Nat. Photon. **15**, 21 (2021), arXiv: 2004.07708.
87 Z. Gong, A. W. Bruch, F. Yang, M. Li, J. Lu, J. B. Surya, C. L. Zou, and H. X. Tang, Opt. Lett. **47**, 746 (2022).
88 K. C. Balram, M. I. Davanço, J. D. Song, and K. Srinivasan, Nat. Photon. **10**, 346 (2016).
89 X. Han, W. Fu, C. Zhong, C. L. Zou, Y. Xu, A. A. Sayem, M. Xu, S. Wang, R. Cheng, L. Jiang, and H. X. Tang, Nat. Commun. **11**, 3237 (2020), arXiv: 2001.09483.
90 T. J. Lu, B. Lienhard, K. Y. Jeong, H. Moon, A. Iranmanesh, G. Grosso, and D. Englund, ACS Photon. **7**, 2650 (2020).
91 D. Zhu, Q. Y. Zhao, H. Choi, T. J. Lu, A. E. Dane, D. Englund, and K. K. Berggren, Nat. Nanotech. **13**, 596 (2018), arXiv: 1711.10546.
92 R. Cheng, J. Wright, H. G. Xing, D. Jena, and H. X. Tang, Appl. Phys. Lett. **117**, 132601 (2020), arXiv: 2006.09643.
93 S. Wang, M. Zhan, G. Wang, H. Xuan, W. Zhang, C. Liu, C. Xu, Y. Liu, Z. Wei, and X. Chen, Laser Photon. Rev. **7**, 831 (2013).
94 R. Adair, L. L. Chase, and S. A. Payne, Phys. Rev. B **39**, 3337 (1989).
95 D. M. Lukin, C. Dory, M. A. Guidry, K. Y. Yang, S. D. Mishra, R. Trivedi, M. Radulaski, S. Sun, D. Vercruysse, G. H. Ahn, and J. Vučković, Nat. Photon. **14**, 330 (2020).
96 D. M. Lukin, M. A. Guidry, and J. Vučković, PRX Quantum **1**, 020102 (2020).
97 A. Bourassa, C. P. Anderson, K. C. Miao, M. Onizhuk, H. Ma, A. L. Crook, H. Abe, J. Ul-Hassan, T. Ohshima, N. T. Son, G. Galli, and D. D. Awschalom, Nat. Mater. **19**, 1319 (2020), arXiv: 2005.07602.
98 C. Wang, Z. Fang, A. Yi, B. Yang, Z. Wang, L. Zhou, C. Shen, Y. Zhu, Y. Zhou, R. Bao, Z. Li, Y. Chen, K. Huang, J. Zhang, Y. Cheng, and X. Ou, Light Sci. Appl. **10**, 139 (2021).
99 A. L. Crook, C. P. Anderson, K. C. Miao, A. Bourassa, H. Lee, S. L. Bayliss, D. O. Bracher, X. Zhang, H. Abe, T. Ohshima, E. L. Hu, and D. D. Awschalom, Nano Lett. **20**, 3427 (2020), arXiv: 2003.00042.
100 C. Wang, C. Shen, A. Yi, S. Yang, L. Zhou, Y. Zhu, K. Huang, S. Song, M. Zhou, J. Zhang, and X. Ou, Opt. Lett. **46**, 2952 (2021), arXiv: 2103.04547.
101 X. Lu, J. Y. Lee, P. X. L. Feng, and Q. Lin, Opt. Lett. **38**, 1304 (2013).
102 B. S. Song, S. Yamada, T. Asano, and S. Noda, Opt. Express **19**, 11084 (2011).
103 A. Yi, Y. Zheng, H. Huang, J. Lin, Y. Yan, T. You, K. Huang, S. Zhang, C. Shen, M. Zhou, W. Huang, J. Zhang, S. Zhou, H. Ou, and X. Ou, Opt. Mater. **107**, 109990 (2020).
104 Y. Zheng, M. Pu, A. Yi, B. Chang, T. You, K. Huang, A. N. Kamel, M. R. Henriksen, A. A. Jørgensen, X. Ou, and H. Ou, Opt. Express **27**, 13053 (2019).
105 T. Fan, H. Moradinejad, X. Wu, A. A. Eftekhar, and A. Adibi, Opt. Express **26**, 25814 (2018).
106 B. S. Song, T. Asano, S. Jeon, H. Kim, C. Chen, D. D. Kang, and S. Noda, Optica **6**, 991 (2019).
107 D. M. Lukin, M. A. Guidry, J. Yang, M. Ghezellou, S. D. Mishra, H. Abe, T. Ohshima, J. Ul-Hassan, and J. Vuovi, arXiv: 2202.04845.
108 M. A. Guidry, D. M. Lukin, K. Y. Yang, R. Trivedi, and J. Vučković, Nat. Photon. **16**, 52 (2022), arXiv: 2103.10517.
109 C. Babin, R. Stöhr, N. Morioka, T. Linkewitz, T. Steidl, R. Wörnle, D. Liu, E. Hesselmeier, V. Vorobyov, A. Denisenko, M. Hentschel, C. Gobert, P. Berwian, G. V. Astakhov, W. Knolle, S. Majety, P. Saha, M. Radulaski, N. T. Son, J. Ul-Hassan, F. Kaiser, and J. Wrachtrup, Nat. Mater. **21**, 67 (2022), arXiv: 2109.04737.
110 D. Zhu, L. Shao, M. Yu, R. Cheng, B. Desiatov, C. J. Xin, Y. Hu, J. Holzgrafe, S. Ghosh, A. Shams-Ansari, E. Puma, N. Sinclair, C. Reimer, M. Zhang, and M. Lončar, Adv. Opt. Photon. **13**, 242 (2021), arXiv: 2102.11956.
111 J. Lin, F. Bo, Y. Cheng, and J. Xu, Photon. Res. **8**, 1910 (2020).
112 J. Zhang, Z. Fang, J. Lin, J. Zhou, M. Wang, R. Wu, R. Gao, and Y. Cheng, Nanomaterials **9**, 1218 (2019).
113 J. Wang, Z. Liu, J. Xiang, B. Chen, Y. Wei, W. Liu, Y. Xu, S. Lan, and J. Liu, Nanophotonics **10**, 4273 (2021).
114 B. Y. Xu, L. K. Chen, J. T. Lin, L. T. Feng, R. Niu, Z. Y. Zhou, R. H.

Gao, C. H. Dong, G. C. Guo, Q. H. Gong, Y. Cheng, Y. F. Xiao, and X. F. Ren, Sci. China-Phys. Mech. Astron. **65**, 294262 (2022).
115 A. Guarino, G. Poberaj, D. Rezzonico, R. Degl'Innocenti, and P. Günter, Nat. Photon. **1**, 407 (2007), arXiv: 0705.2392.
116 J. Wang, F. Bo, S. Wan, W. Li, F. Gao, J. Li, G. Zhang, and J. Xu, Opt. Express **23**, 23072 (2015).
117 M. Zhang, C. Wang, R. Cheng, A. Shams-Ansari, and M. Lončar, Optica **4**, 1536 (2017), arXiv: 1712.04479.
118 R. Wu, J. Zhang, N. Yao, W. Fang, L. Qiao, Z. Chai, J. Lin, and Y. Cheng, Opt. Lett. **43**, 4116 (2018), arXiv: 1806.00099.
119 Z. Hao, J. Wang, S. Ma, W. Mao, F. Bo, F. Gao, G. Zhang, and J. Xu, Photon. Res. **5**, 623 (2017).
120 Z. Z. Hao, L. Zhang, A. Gao, W. B. Mao, X. D. Lyu, X. M. Gao, F. Bo, F. Gao, G. Q. Zhang, and J. J. Xu, Sci. China-Phys. Mech. Astron. **61**, 114211 (2018).
121 J. Lin, N. Yao, Z. Hao, J. Zhang, W. Mao, M. Wang, W. Chu, R. Wu, Z. Fang, L. Qiao, W. Fang, F. Bo, and Y. Cheng, Phys. Rev. Lett. **122**, 173903 (2019).
122 J. Lu, J. B. Surya, X. Liu, A. W. Bruch, Z. Gong, Y. Xu, and H. X. Tang, Optica **6**, 1455 (2019), arXiv: 1911.00083.
123 J. Y. Chen, Z. H. Ma, Y. M. Sua, Z. Li, C. Tang, and Y. P. Huang, Optica **6**, 1244 (2019).
124 J. Lu, M. Li, C. L. Zou, A. Al Sayem, and H. X. Tang, Optica **7**, 1654 (2020), arXiv: 2007.07411.
125 R. Wolf, I. Breunig, H. Zappe, and K. Buse, Opt. Express **25**, 29927 (2017).
126 Z. Ma, J. Y. Chen, Z. Li, C. Tang, Y. M. Sua, H. Fan, and Y. P. Huang, Phys. Rev. Lett. **125**, 263602 (2020), arXiv: 2010.04242.
127 Y. He, Q. F. Yang, J. Ling, R. Luo, H. Liang, M. Li, B. Shen, H. Wang, K. Vahala, and Q. Lin, Optica **6**, 1138 (2019), arXiv: 1812.09610.
128 M. Zhang, B. Buscaino, C. Wang, A. Shams-Ansari, C. Reimer, R. Zhu, J. M. Kahn, and M. Lončar, Nature **568**, 373 (2019), arXiv: 1809.08636.
129 Z. Wang, Z. Fang, Z. Liu, W. Chu, Y. Zhou, J. Zhang, R. Wu, M. Wang, T. Lu, and Y. Cheng, Opt. Lett. **46**, 380 (2021).
130 Y. A. Liu, X. S. Yan, J. W. Wu, B. Zhu, Y. P. Chen, and X. F. Chen, Sci. China-Phys. Mech. Astron. **64**, 234262 (2021), arXiv: 2009.12900.
131 Q. Luo, Z. Z. Hao, C. Yang, R. Zhang, D. H. Zheng, S. G. Liu, H. D. Liu, F. Bo, Y. F. Kong, G. Q. Zhang, and J. J. Xu, Sci. China-Phys. Mech. Astron. **64**, 234263 (2021).
132 Y. Zhou, Z. Wang, Z. Fang, Z. Liu, H. Zhang, D. Yin, Y. Liang, Z. Zhang, J. Liu, T. Huang, R. Bao, R. Wu, J. Lin, M. Wang, and Y. Cheng, Opt. Lett. **46**, 5651 (2021), arXiv: 2108.06003.
133 T. Li, K. Wu, M. Cai, Z. Xiao, H. Zhang, C. Li, J. Xiang, Y. Huang, and J. Chen, APL Photon. **6**, 101301 (2021), arXiv: 2106.11666.
134 R. Zhang, C. Yang, Z. Z. Hao, D. Jia, Q. Luo, D. H. Zheng, H. D. Liu, X. Y. Yu, F. Gao, F. Bo, Y. F. Kong, G. Q. Zhang, and J. J. Xu, Sci. China-Phys. Mech. Astron. **64**, 294216 (2021), arXiv: 2106.04933.
135 R. W. Boyd, *Nonlinear Optics* (Academic Press, San Diego, 2008).
136 S. Calvez, G. Lafleur, A. Larrue, P. F. Calmon, A. Arnoult, G. Almuneau, and O. Gauthier-Lafaye, IEEE Photon. Technol. Lett. **27**, 982 (2015).
137 C. Ozanam, M. Savanier, L. Lanco, X. Lafosse, A. Andronico, I. Favero, S. Ducci, and G. Leo, in *Near-infrared OPO in an AlGaAs/AlOx waveguide: Proceedings of the Quantum Sensing and Nanophotonic Devices XI* (SPIE, San Francisco, 2014), Vol. 8993, p. 899306.
138 M. R. Krames, A. D. Minervini, and N. Holonyak Jr., Appl. Phys. Lett. **67**, 73 (1995).
139 P. Jiang, and K. C. Balram, Opt. Express **28**, 12262 (2020), arXiv: 1912.05301.
140 B. Guha, F. Marsault, F. Cadiz, L. Morgenroth, V. Ulin, V. Berkovitz, A. Lemare, C. Gomez, A. Amo, S. Combrié, B. Gérard, G. Leo, and I. Favero, Optica **4**, 218 (2017), arXiv: 1605.00477.
141 P. S. Kuo, J. Bravo-Abad, and G. S. Solomon, Nat. Commun. **5**, 3109 (2014).
142 M. Pu, L. Ottaviano, E. Semenova, and K. Yvind, Optica **3**, 823 (2016).
143 L. Chang, W. Xie, H. Shu, Q. F. Yang, B. Shen, A. Boes, J. D. Peters, W. Jin, C. Xiang, S. Liu, G. Moille, S. P. Yu, X. Wang, K. Srinivasan, S. B. Papp, K. Vahala, and J. E. Bowers, Nat. Commun. **11**, 1331 (2020), arXiv: 1909.09778.
144 L. Chang, A. Boes, P. Pintus, J. D. Peters, M. J. Kennedy, X. W. Guo, N. Volet, S. P. Yu, S. B. Papp, and J. E. Bowers, APL Photon. **4**, 036103 (2019).
145 L. Chang, A. Boes, X. Guo, D. T. Spencer, M. J. Kennedy, J. D. Peters, N. Volet, J. Chiles, A. Kowligy, N. Nader, D. D. Hickstein, E. J. Stanton, S. A. Diddams, S. B. Papp, and J. E. Bowers, Laser Photon. Rev. **12**, 1800149 (2018), arXiv: 1805.09379.
146 W. Xie, L. Chang, H. Shu, J. C. Norman, J. D. Peters, X. Wang, and J. E. Bowers, Opt. Express **28**, 32894 (2020), arXiv: 2004.14537.
147 H. Shu, L. Chang, C. Lao, B. Shen, W. Xie, X. Zhang, M. Jin, Y. Tao, R. Chen, Z. Tao, S. Yu, Q.-F. Yang, X. Wang, and J. E. Bowers, arXiv: 2112.08904.
148 T. J. Steiner, J. E. Castro, L. Chang, Q. Dang, W. Xie, J. Norman, J. E. Bowers, and G. Moody, PRX Quantum **2**, 010337 (2021).
149 K. Fang, and M. Zhao, arXiv: 2105.12705.
150 L. Chang, G. D. Cole, G. Moody, and J. E. Bowers, Opt. Photon. News **33**, 24 (2022).
151 R. Zhang, J. Fan, X. Zhang, H. Yu, H. Zhang, Y. Mai, T. Xu, J. Wang, and H. J. Snaith, ACS Photon. **3**, 371 (2016).
152 G. Xing, N. Mathews, S. S. Lim, N. Yantara, X. Liu, D. Sabba, M. Grätzel, S. Mhaisalkar, and T. C. Sum, Nat. Mater. **13**, 476 (2014).
153 H. Min, D. Y. Lee, J. Kim, G. Kim, K. S. Lee, J. Kim, M. J. Paik, Y. K. Kim, K. S. Kim, M. G. Kim, T. J. Shin, and S. Il Seok, Nature **598**, 444 (2021).
154 D. Ma, K. Lin, Y. Dong, H. Choubisa, A. H. Proppe, D. Wu, Y. K. Wang, B. Chen, P. Li, J. Z. Fan, F. Yuan, A. Johnston, Y. Liu, Y. Kang, Z. H. Lu, Z. Wei, and E. H. Sargent, Nature **599**, 594 (2021).
155 H. Cha, S. Bae, M. Lee, and H. Jeon, Appl. Phys. Lett. **108**, 181104 (2016).
156 M. Saliba, S. M. Wood, J. B. Patel, P. K. Nayak, J. Huang, J. A. Alexander-Webber, B. Wenger, S. D. Stranks, M. T. Hörantner, J. T. W. Wang, R. J. Nicholas, L. M. Herz, M. B. Johnston, S. M. Morris, H. J. Snaith, and M. K. Riede, Adv. Mater. **28**, 923 (2016).
157 B. R. Sutherland, S. Hoogland, M. M. Adachi, C. T. O. Wong, and E. H. Sargent, ACS Nano **8**, 10947 (2014).
158 K. Wang, G. Xing, Q. Song, and S. Xiao, Adv. Mater. **33**, 2000306 (2021).
159 N. Zhang, W. Sun, S. P. Rodrigues, K. Wang, Z. Gu, S. Wang, W. Cai, S. Xiao, and Q. Song, Adv. Mater. **29**, 1606205 (2017).
160 P. J. Cegielski, A. L. Giesecke, S. Neutzner, C. Porschatis, M. Gandini, D. Schall, C. A. R. Perini, J. Bolten, S. Suckow, S. Kataria, B. Chmielak, T. Wahlbrink, A. Petrozza, and M. C. Lemme, Nano Lett. **18**, 6915 (2018), arXiv: 1907.08058.
161 S. Wang, Y. Liu, G. Li, J. Zhang, N. Zhang, S. Xiao, and Q. Song, Adv. Opt. Mater. **6**, 1701266 (2018).
162 Y. Gao, C. Huang, C. Hao, S. Sun, L. Zhang, C. Zhang, Z. Duan, K. Wang, Z. Jin, N. Zhang, A. V. Kildishev, C. W. Qiu, Q. Song, and S. Xiao, ACS Nano **12**, 8847 (2018).
163 Y. Fan, Y. Wang, N. Zhang, W. Sun, Y. Gao, C. W. Qiu, Q. Song, and S. Xiao, Nat. Commun. **10**, 2085 (2019).
164 C. Huang, C. Zhang, S. Xiao, Y. Wang, Y. Fan, Y. Liu, N. Zhang, G. Qu, H. Ji, J. Han, L. Ge, Y. Kivshar, and Q. Song, Science **367**, 1018 (2020).
165 J. Tian, G. Adamo, H. Liu, M. Klein, S. Han, H. Liu, and C. Soci, Adv. Mater. **34**, 2109157 (2022).
166 F. Xia, H. Wang, D. Xiao, M. Dubey, and A. Ramasubramaniam, Nat. Photon. **8**, 899 (2014), arXiv: 1410.3882.
167 T. Tan, X. Jiang, C. Wang, B. Yao, and H. Zhang, Adv. Sci. **7**, 2000058 (2020).
168 M. Zhu, Y. Zhao, Q. Feng, H. Lu, S. Zhang, N. Zhang, C. Ma, J. Li, J. Zheng, J. Zhang, H. Xu, T. Zhai, and J. Zhao, Small **15**, 1903159

(2019).
169 Z. Liu, J. Wang, B. Chen, Y. Wei, W. Liu, and J. Liu, Nano Lett. **21**, 7405 (2021).
170 I. Datta, S. H. Chae, G. R. Bhatt, M. A. Tadayon, B. Li, Y. Yu, C. Park, J. Park, L. Cao, D. N. Basov, J. Hone, and M. Lipson, Nat. Photon. **14**, 256 (2020), arXiv: 1906.00459.
171 J. H. Chen, Y. F. Xiong, F. Xu, and Y. Q. Lu, Light Sci. Appl. **10**, 78 (2021).
172 L. Wang, X. Zhou, S. Yang, G. Huang, and Y. Mei, Photon. Res. **7**, 905 (2019).
173 Y. Liu, Y. Huang, and X. Duan, Nature **567**, 323 (2019).
174 B. Yao, Y. Liu, S. W. Huang, C. Choi, Z. Xie, J. Flor Flores, Y. Wu, M. Yu, D. L. Kwong, Y. Huang, Y. Rao, X. Duan, and C. W. Wong, Nat. Photon. **12**, 22 (2018), arXiv: 1710.01940.
175 Y. Guo, B. Han, J. Du, S. Cao, H. Gao, N. An, C. Qin, Y. Li, Y, Rao, and B. Yao, in *Kilometers long graphene coated optical fibers for fast temperature sensing: Proceedings of the 2020 Asia Communications and Photonics Conference (ACP) and International Conference on Information Photonics and Optical Communications (IPOC)* (Beijing, 2020).
176 C. T. Phare, Y. H. Daniel Lee, J. Cardenas, and M. Lipson, Nat. Photon. **9**, 511 (2015).
177 B. Yao, S. W. Huang, Y. Liu, A. K. Vinod, C. Choi, M. Hoff, Y. Li, M. Yu, Z. Feng, D. L. Kwong, Y. Huang, Y. Rao, X. Duan, and C. W. Wong, Nature **558**, 410 (2018).
178 J. He, I. Paradisanos, T. Liu, A. R. Cadore, J. Liu, M. Churaev, R. N. Wang, A. S. Raja, C. Javerzac-Galy, P. Roelli, D. D. Fazio, B. L. T. Rosa, S. Tongay, G. Soavi, A. C. Ferrari, and T. J. Kippenberg, Nano Lett. **21**, 2709 (2021), arXiv: 2010.06014.
179 B. Yao, C. Yu, Y. Wu, S. W. Huang, H. Wu, Y. Gong, Y. Chen, Y. Li, C. W. Wong, X. Fan, and Y. Rao, Nano Lett. **17**, 4996 (2017).
180 Z. Cao, B. Yao, C. Qin, R. Yang, Y. Guo, Y. Zhang, Y. Wu, L. Bi, Y. Chen, Z. Xie, G. Peng, S. W. Huang, C. W. Wong, and Y. Rao, Light Sci. Appl. **8**, 107 (2019).
181 C. Javerzac-Galy, A. Kumar, R. D. Schilling, N. Piro, S. Khorasani, M. Barbone, I. Goykhman, J. B. Khurgin, A. C. Ferrari, and T. J. Kippenberg, Nano Lett. **18**, 3138 (2018), arXiv: 1710.04294.
182 T. Tan, Z. Yuan, H. Zhang, G. Yan, S. Zhou, N. An, B. Peng, G. Soavi, Y. Rao, and B. Yao, Nat. Commun. **12**, 6716 (2021).
183 Y. Ye, Z. J. Wong, X. Lu, X. Ni, H. Zhu, X. Chen, Y. Wang, and X. Zhang, Nat. Photon. **9**, 733 (2015), arXiv: 1503.06141.
184 T. Ren, P. Song, J. Chen, and K. P. Loh, ACS Photon. **5**, 353 (2018).
185 A. Martinez, and S. Yamashita, Appl. Phys. Lett. **101**, 041118 (2012).
186 C. Qin, K. Jia, Q. Li, T. Tan, X. Wang, Y. Guo, S. W. Huang, Y. Liu, S. Zhu, Z. Xie, Y. Rao, and B. Yao, Light Sci. Appl. **9**, 185 (2020).
187 Y. Guo, N. An, K. Guo, Y. Li, Y. Liang, C. Wu, Y. Wang, J. He, Y. Wang, T. Tan, Y. Rao, and B. Yao, Sens. Actuat. B-Chem. **348**, 130694 (2021).
188 J. M. Hales, J. Matichak, S. Barlow, S. Ohira, K. Yesudas, J. L. Brédas, J. W. Perry, and S. R. Marder, Science **327**, 1485 (2010).
189 D. L. Elder, and L. R. Dalton, Ind. Eng. Chem. Res. **61**, 1207 (2022).
190 G. W. Lu, J. Hong, F. Qiu, A. M. Spring, T. Kashino, J. Oshima, M. A. Ozawa, H. Nawata, and S. Yokoyama, Nat. Commun. **11**, 4224 (2020).
191 X. Hu, P. Jiang, C. Ding, H. Yang, and Q. Gong, Nat. Photon. **2**, 185 (2008).
192 C. Koos, P. Vorreau, T. Vallaitis, P. Dumon, W. Bogaerts, R. Baets, B. Esembeson, I. Biaggio, T. Michinobu, F. Diederich, W. Freude, and J. Leuthold, Nat. Photon. **3**, 216 (2009).
193 Y. Wang, S. He, X. Gao, P. Ye, L. Lei, W. Dong, X. Zhang, and P. Xu, Photon. Res. **10**, 50 (2022).
194 X. Shen, R. C. Beltran, V. M. Diep, S. Soltani, and A. M. Armani, Sci. Adv. **4**, eaao4507 (2018).
195 J. H. Chen, X. Shen, S. J. Tang, Q. T. Cao, Q. Gong, and Y. F. Xiao, Phys. Rev. Lett. **123**, 173902 (2019).
196 Y. Enami, C. T. Derose, D. Mathine, C. Loychik, C. Greenlee, R. A. Norwood, T. D. Kim, J. Luo, Y. Tian, A. K. Y. Jen, and N. Peyghambarian, Nat. Photon. **1**, 180 (2007).
197 A. W. Zhou, and J. Y. Fan, Sci. China Math. **58**, 1 (2015).
198 F. Gu, F. Xie, X. Lin, S. Linghu, W. Fang, H. Zeng, L. Tong, and S. Zhuang, Light Sci. Appl. **6**, e17061 (2017).
199 X. Jiang, and L. Yang, Light Sci. Appl. **9**, 24 (2020), arXiv: 1911.06789.
200 T. Grossmann, S. Klinkhammer, M. Hauser, D. Floess, T. Beck, C. Vannahme, T. Mappes, U. Lemmer, and H. Kalt, Opt. Express **19**, 10009 (2011).
201 D. Chen, A. Kovach, X. Shen, S. Poust, and A. M. Armani, ACS Photon. **4**, 2376 (2017).
202 X. Zhang, H. Luo, W. Xiong, X. Chen, X. Han, G. Xiao, and H. Feng, Phys. Rev. A **103**, 023515 (2021).
203 X. Shen, H. Choi, D. Chen, W. Zhao, and A. M. Armani, Nat. Photon. **14**, 95 (2020), arXiv: 1911.07777.
204 L. H. Gao, X. Chen, S. Lu, and K. Z. Wang, J. Nanosci. Nanotech. **14**, 3808 (2014).
205 N. Peor, R. Sfez, and S. Yitzchaik, J. Am. Chem. Soc. **130**, 4158 (2008).
206 B. J. M. Hausmann, I. Bulu, V. Venkataraman, P. Deotare, and M. Lončar, Nat. Photon. **8**, 369 (2014).
207 J. Wang, F. Sciarrino, A. Laing, and M. G. Thompson, Nat. Photon. **14**, 273 (2020), arXiv: 2005.01948.
208 M. W. Doherty, N. B. Manson, P. Delaney, F. Jelezko, J. Wrachtrup, and L. C. L. Hollenberg, Phys. Rep. **528**, 1 (2013), arXiv: 1302.3288.
209 C. Bradac, W. Gao, J. Forneris, M. E. Trusheim, and I. Aharonovich, Nat. Commun. **10**, 5625 (2019).
210 M. K. Bhaskar, D. D. Sukachev, A. Sipahigil, R. E. Evans, M. J. Burek, C. T. Nguyen, L. J. Rogers, P. Siyushev, M. H. Metsch, H. Park, F. Jelezko, M. Lončar, and M. D. Lukin, Phys. Rev. Lett. **118**, 223603 (2017), arXiv: 1612.03036.
211 P. Siyushev, M. H. Metsch, A. Ijaz, J. M. Binder, M. K. Bhaskar, D. D. Sukachev, A. Sipahigil, R. E. Evans, C. T. Nguyen, M. D. Lukin, P. R. Hemmer, Y. N. Palyanov, I. N. Kupriyanov, Y. M. Borzdov, L. J. Rogers, and F. Jelezko, Phys. Rev. B **96**, 081201 (2017), arXiv: 1612.02947.
212 K. Bray, B. Regan, A. Trycz, R. Previdi, G. Seniutinas, K. Ganesan, M. Kianinia, S. Kim, and I. Aharonovich, ACS Photon. **5**, 4817 (2018).
213 M. Nguyen, N. Nikolay, C. Bradac, M. Kianinia, E. A. Ekimov, N. Mendelson, O. Benson, and I. Aharonovich, Adv. Photon. **1**, 1 (2019).
214 T. T. Toan, B. Regan, and C. Bradac, in *CLEO: Science and Innovations: Proceedings Conference on Lasers and Electro-Optics Part of CLEO: 2019*, San Jose, 2019
215 A. Trycz, B. Regan, M. Kianinia, K. Bray, M. Toth, and I. Aharonovich, Opt. Mater. Express **9**, 4708 (2019).
216 M. J. Burek, C. Meuwly, R. E. Evans, M. K. Bhaskar, A. Sipahigil, S. Meesala, B. Machielse, D. D. Sukachev, C. T. Nguyen, J. L. Pacheco, E. Bielejec, M. D. Lukin, and M. Lončar, Phys. Rev. Appl. **8**, 024026 (2017), arXiv: 1612.05285.
217 S. Häußler, J. Benedikter, K. Bray, B. Regan, A. Dietrich, J. Twamley, I. Aharonovich, D. Hunger, and A. Kubanek, Phys. Rev. B **99**, 165310 (2019), arXiv: 1812.02426.
218 E. Janitz, M. Ruf, Y. Fontana, J. Sankey, and L. Childress, Opt. Express **25**, 20932 (2017).
219 D. Milewska, K. Karpienko, and M. Jędrzejewska-Szczerska, Diamond Relat. Mater. **64**, 169 (2016).
220 P. Latawiec, V. Venkataraman, M. J. Burek, B. J. M. Hausmann, I. Bulu, and M. Lončar, Optica **2**, 924 (2015), arXiv: 1509.00373.
221 Z. Tian, P. Zhang, and X. W. Chen, Phys. Rev. Appl. **15**, 054043 (2021).
222 I. Aharonovich, J. C. Lee, A. P. Magyar, B. B. Buckley, C. G. Yale, D. D. Awschalom, and E. L. Hu, Adv. Mater. **24**, OP54 (2012).
223 P. Hill, E. Gu, M. D. Dawson, and M. J. Strain, Diamond Relat. Mater. **88**, 215 (2018).

224 A. Butcher, X. Guo, R. Shreiner, N. Delegan, K. Hao, I. Duda Peter J., D. D. Awschalom, F. J. Heremans, and A. A. High, Nano Lett. **20**, 4603 (2020), arXiv: 2004.03532.

225 M. Challier, S. Sonusen, A. Barfuss, D. Rohner, D. Riedel, J. Koelbl, M. Ganzhorn, P. Appel, P. Maletinsky, and E. Neu, Micromachines **9**, 148 (2018).

226 J. C. Lee, A. P. Magyar, D. O. Bracher, I. Aharonovich, and E. L. Hu, Diamond Relat. Mater. **33**, 45 (2013), arXiv: 1210.0125.

227 A. P. Magyar, J. C. Lee, A. M. Limarga, I. Aharonovich, F. Rol, D. R. Clarke, M. Huang, and E. L. Hu, Appl. Phys. Lett. **99**, 081913 (2011), arXiv: 1108.0738.

228 B. Regan, S. Kim, A. T. H. Ly, A. Trycz, K. Bray, K. Ganesan, M. Toth, and I. Aharonovich, InfoMat **2**, 1241 (2020).

229 D. Englund, B. Shields, K. Rivoire, F. Hatami, J. Vučković, H. Park, and M. D. Lukin, Nano Lett. **10**, 3922 (2010), arXiv: 1005.2204.

230 T. Gaebel, M. Domhan, I. Popa, C. Wittmann, P. Neumann, F. Jelezko, J. R. Rabeau, N. Stavrias, A. D. Greentree, S. Prawer, J. Meijer, J. Twamley, P. R. Hemmer, and J. Wrachtrup, Nat. Phys. **2**, 408 (2006), arXiv: quant-ph/0605038.

231 S. Johnson, P. R. Dolan, T. Grange, A. A. P. Trichet, G. Hornecker, Y. C. Chen, L. Weng, G. M. Hughes, A. A. R. Watt, A. Auffèves, and J. M. Smith, New J. Phys. **17**, 122003 (2015), arXiv: 1506.05161.

232 K. Kuruma, B. Pingault, C. Chia, D. Renaud, P. Hoffmann, S. Iwamoto, C. Ronning, and M. Lončar, Appl. Phys. Lett. **118**, 230601 (2021), arXiv: 2105.01715.

233 J. C. Lee, D. O. Bracher, S. Cui, K. Ohno, C. A. McLellan, X. Zhang, P. Andrich, B. Alemán, K. J. Russell, A. P. Magyar, I. Aharonovich, A. Bleszynski Jayich, D. Awschalom, and E. L. Hu, Appl. Phys. Lett. **105**, 261101 (2014), arXiv: 1411.0725.

234 J. Riedrich-Möller, C. Arend, C. Pauly, F. Mücklich, M. Fischer, S. Gsell, M. Schreck, and C. Becher, Nano Lett. **14**, 5281 (2014), arXiv: 1408.1803.

235 N. H. Wan, T.-J. Lu, K. C. Chen, M. P. Walsh, M. E. Trusheim, L. De Santis, E. A. Bersin, I. B. Harris, S. L. Mouradian, I. R. Christen, E. S. Bielejec, and D. Englund, Nature **583**, 226 (2020).

236 P. E. Barclay, C. Santori, K. M. Fu, R. G. Beausoleil, and O. Painter, Opt. Express **17**, 8081 (2009), arXiv: 0812.4505.

237 M. E. Trusheim, B. Pingault, N. H. Wan, M. Gündoğan, L. De Santis, R. Debroux, D. Gangloff, C. Purser, K. C. Chen, M. Walsh, J. J. Rose, J. N. Becker, B. Lienhard, E. Bersin, I. Paradeisanos, G. Wang, D. Lyzwa, A. R. P. Montblanch, G. Malladi, H. Bakhru, A. C. Ferrari, I. A. Walmsley, M. Atatüre, and D. Englund, Phys. Rev. Lett. **124**, 023602 (2020).

238 Y. Zhou, A. Rasmita, K. Li, Q. Xiong, I. Aharonovich, and W. B. Gao, Nat. Commun. **8**, 14451 (2017), arXiv: 1610.00882.

239 X. Zhu, S. Saito, A. Kemp, K. Kakuyanagi, S. I. Karimoto, H. Nakano, W. J. Munro, Y. Tokura, M. S. Everitt, K. Nemoto, M. Kasu, N. Mizuochi, and K. Semba, Nature **478**, 221 (2011), arXiv: 1111.5399.

240 C. Dory, D. Vercruysse, K. Y. Yang, N. V. Sapra, A. E. Rugar, S. Sun, D. M. Lukin, A. Y. Piggott, J. L. Zhang, M. Radulaski, K. G. Lagoudakis, L. Su, and J. Vuč ković, Nat. Commun. **10**, 3309 (2019).

241 S. Castelletto, L. Rosa, J. Blackledge, M. Z. Al Abri, and A. Boretti, Microsyst. Nanoeng. **3**, 17061 (2017).

242 P. Latawiec, M. J. Burek, Y. I. Sohn, and M. Lončar, J. Vacuum Sci. Tech. B **34**, 041801 (2020).

243 S. Mi, M. Kiss, T. Graziosi, and N. Quack, J. Phys. Photon. **2**, 042001 (2020).

244 A. H. Piracha, P. Rath, K. Ganesan, S. Kühn, W. H. P. Pernice, and S. Prawer, Nano Lett. **16**, 3341 (2016).

245 M. Radtke, R. Nelz, A. Slablab, and E. Neu, Micromachines **10**, 718 (2019).

246 D. Rani, O. R. Opaluch, and E. Neu, Micromachines **12**, 36 (2021).

247 B. Regan, A. Trycz, J. E. Fröch, O. C. Schaeper, S. Kim, and I. Aharonovich, Nanoscale **13**, 8848 (2021).

248 Y. Tao, J. M. Boss, B. A. Moores, and C. L. Degen, Nat. Commun. **5**, 3638 (2014), arXiv: 1212.1347.

249 L. Li, I. Bayn, M. Lu, C. Y. Nam, T. Schröder, A. Stein, N. C. Harris, and D. Englund, Sci. Rep. **5**, 7802 (2015).

250 A. Faraon, P. E. Barclay, C. Santori, K. M. C. Fu, and R. G. Beausoleil, Nat. Photon. **5**, 301 (2011), arXiv: 1012.3815.

251 J. Liu, H. Tian, E. Lucas, A. S. Raja, G. Lihachev, R. N. Wang, J. He, T. Liu, M. H. Anderson, W. Weng, S. A. Bhave, and T. J. Kippenberg, Nature **583**, 385 (2020), arXiv: 1912.08686.

252 C. Qiu, B. Wang, N. Zhang, S. Zhang, J. Liu, D. Walker, Y. Wang, H. Tian, T. R. Shrout, Z. Xu, L. Q. Chen, and F. Li, Nature **577**, 350 (2020).